Atmos. Chem. Phys. Discuss., 4, 6379–6430, 2004
www.atmos-chem-phys.org/acpd/4/6379/
SRef-ID: 1680-7375/acpd/2004-4-6379

Atmospheric Chemistry and Physics Discussions

Parametric sensitivity and uncertainty analysis of dimethylsulfide oxidation in the remote marine boundary layer

D. D. Lucas[1, *] **and R. G. Prinn**[1]

[1]Department of Earth, Atmospheric, and Planetary Sciences, MIT, Cambridge, MA 02139, USA
[*]Present address: Frontier Research Center for Global Change, Yokohama, Japan

Received: 18 August 2004 – Accepted: 23 September 2004 – Published: 7 October 2004

Correspondence to: D. D. Lucas (ddlucas@alum.mit.edu)

Abstract

A study of the current significant uncertainties in dimethylsulfide (DMS) gas-phase chemistry provides insight into additional research needed to decrease these uncertainties. The DMS oxidation cycle in the remote marine boundary layer is simulated using a diurnally-varying box model with 56 uncertain chemical and physical parameters. Two analytical methods (direct integration and probabilistic collocation) are used to determine the most influential parameters (sensitivity analysis) and sources of uncertainty (uncertainty analysis) affecting the concentrations of DMS, SO_2, methanesulfonic acid (MSA), and H_2SO_4. The key parameters identified by the sensitivity analysis are associated with DMS emissions, mixing in to and out of the boundary layer, heterogeneous removal of soluble sulfur-containing compounds, and the DMS+OH addition and abstraction reactions. MSA and H_2SO_4 are also sensitive to the rate constants of numerous other reactions, which limits the effectiveness of mechanism reduction techniques. Propagating the parameter uncertainties through the model leads to concentrations that are uncertain by factors of 1.8 to 3.0. The main sources of uncertainty are from DMS emissions and heterogeneous scavenging. Uncertain chemical rate constants, however, collectively account for up to 50–60% of the net uncertainties in MSA and H_2SO_4. The concentration uncertainties are also calculated at different temperatures, where they vary mainly due to temperature-dependent chemistry. With changing temperature, the uncertainties of DMS and SO_2 remain steady, while the uncertainties of MSA and H_2SO_4 vary by factors of 2 to 4.

1. Introduction

The production of dimethylsulfide (CH_3SCH_3, DMS) by marine phytoplankton (Keller et al., 1989) is believed to be the largest source of natural sulfur to the global atmosphere (Bates et al., 1992). In the atmosphere DMS is photochemically oxidized to a multitude of sulfur-bearing species, many of which have an affinity for interacting with

ACPD

4, 6379–6430, 2004

Sensitivities and uncertainties of DMS oxidation in the RMBL

D. D. Lucas and R. G. Prinn

existing, or creating new, aerosols. These connections form part of a proposed feedback whereby DMS may influence climate and radiation on a planetary scale (Shaw, 1983; Charlson et al., 1987). Although the proposed DMS-climate link has sparked extensive research (Restelli and Angeletti, 1993; Andreae and Crutzen, 1997), many large sources of uncertainty still remain. Two widely used sea-air transfer velocities, for instance, yield DMS fluxes that differ by a factor of two (Liss and Merlivat, 1986; Wanninkhof, 1992). As another example, the formation rates of new sulfate aerosols differ by an order of magnitude between two recent studies (Kulmala et al., 1998; Verheggen and Mozurkewich, 2002).

Another recognized, but not well quantified, source of uncertainty arises from the gas-phase oxidation of DMS. The oxidation steps involve many species, competing reactions, and multiple branch points (Yin et al., 1990; Turnipseed and Ravishankara, 1993; Urbanski and Wine, 1999; Lucas and Prinn, 2002). Only a small number of the DMS-related rate constants have been measured in the laboratory, so the majority are estimated as highly uncertain. Quantifying the effects of these uncertain chemical reactions on predictions of the sulfur-containing species is therefore vital. Moreover, it is critical to rank the uncertain DMS chemistry relative to uncertain non-photochemical processes (e.g. DMS emissions and heterogeneous scavenging). A quantitative comparison of these uncertainties is reported here, with the goal of stimulating further research into the relevant areas. We carry out this analysis by applying parametric sensitivity and uncertainty techniques to the DMS oxidation cycle in the remote marine boundary layer (RMBL).

Few sensitivity and uncertainty studies have been performed on systems containing comprehensive DMS oxidation chemistry. In one recent study, Capaldo and Pandis (1997) calculated the sensitivities of the DMS-related concentrations to chemical and physical parameters for different mechanisms in a RMBL box model. Their model predictions were particularly sensitive to the parameters associated with DMS emissions, heterogeneous processes, and vertical mixing. Their study, however, did not consider sensitivities to rate constants and the propagation of rate constant uncertainties to the

ACPD
4, 6379–6430, 2004

species concentrations. Furthermore, as noted by Saltelli (1999), Capaldo and Pandis (1997) applied a sensitivity technique that was unable to capture parameter interactions affecting the sulfur-bearing compounds.

In another study, Saltelli and Hjorth (1995) computed the sensitivities and uncertainties of ratios of important sulfur-containing end products to the kinetic parameters in a moderately complex DMS mechanism. Extensions of this work appeared subsequently in Campolongo et al. (1999) and Saltelli (1999). Using Monte Carlo and regression analyses, Saltelli and Hjorth (1995) explicitly accounted for system non-linearities by sampling the uncertainty spaces of the rate constants. Contingent upon their model structure, they identified and ranked the most important kinetic parameters. Their model, however, lacked important non-photochemical processes (e.g. DMS emissions and heterogeneous scavenging), so they could not rank the relative importance of uncertainties in DMS chemistry versus physical processes. Moreover, their model did not include diurnal variations that are known to play a large role in the DMS cycle in the RMBL (e.g. they used constant OH levels).

In this report, we bridge the gaps in these previous studies by using a diurnally-varying model of the DMS cycle in the RMBL that contains both comprehensive chemistry and physical processes. Through a rigorous sensitivity and uncertainty analysis, we identify the most influential processes affecting the concentrations and concentration uncertainties of the DMS-related compounds. A parametric analysis is our focus because external conditions (e.g. temperature and pressure) are typically much better known than the DMS-related parameters. Because the DMS cycle is time-dependent, complex, and potentially non-linear, we use two separate analytical methods. One is a standard direct integration method that computes the first-order concentration sensitivities and uncertainties as a function of time (Dickinson and Gelinas, 1976; Leis and Kramer, 1988a). The other is the probabilistic collocation method (Tatang et al., 1997) which analyzes higher-order sensitivities and uncertainty contributions from pairs of parameters. Given the extreme impact of temperature on branching in the DMS oxidation mechanism, we also examine the concentration uncertainties across a range of

ACPD
4, 6379–6430, 2004

temperatures.

2. DMS chemistry in the RMBL

2.1. Model description and processes

Figure 1 illustrates the major processes affecting the gas-phase DMS-related species in the RMBL. We describe these processes using coupled ordinary differential equations (ODEs) of the form

$$\frac{dn_i}{dt} = f_i(n, p_c) - p_{h,i} n_i + p_m(n_{f,i} - n_i) + p_{e,i}, \quad (1)$$

where n_i and $n_{f,i}$ are the number concentrations of sulfur-based species i in the RMBL and free troposphere, respectively, f is the net chemical production function, and the p's are the process parameters. Specifically, p_c represents the gas-phase chemical reaction rate constants, p_h is the first-order heterogeneous removal, p_m is associated with the parameterized mixing, and p_e is the oceanic emissions source. As shown in Table 1, our DMS model includes 25 sulfur-based species and 56 uncertain parameters (47 gas phase and 9 non-gas phase). 1D and 3D models containing variations of this DMS chemistry have been previously described (Lucas and Prinn, 2002; Lucas, 2003; Lucas and Prinn, 2003). Note that we use a structurally simple model to ensure numerical efficiency required for the numerous model runs in the sensitivity and uncertainty analysis. Though structurally simple, similar models have been used to estimate DMS surface fluxes and heterogeneous removal rates, and for comparisons with field observations (Davis et al., 1999; Chen et al., 2000; Shon et al., 2001). Our study focuses mainly on the highly uncertain gas-phase DMS chemistry. An additional set of uncertainties pertains to aqueous phase chemistry and cloud microphysics and dynamics, which will require attention in future studies.

ACPD
4, 6379–6430, 2004

2.1.1. Gas-phase DMS chemistry

The gas-phase oxidation of DMS is calculated using a comprehensive mechanism containing 47 sulfur-containing reactions. In addition to DMS, this mechanism represents dimethylsulfoxide (DMSO, $CH_3S(O)CH_3$), dimethylsulfone ($DMSO_2$, $CH_3S(O)_2CH_3$), sulfur dioxide (SO_2), sulfuric acid (H_2SO_4), methanesulfenic acid (MSEA, CH_3SOH), methanesulfinic acid (MSIA, $CH_3S(O)OH$), and methanesulfonic acid (MSA, CH_3SO_3H). This scheme is derived from Lucas and Prinn (2002), where it yielded levels of DMS, SO_2, MSA, and H_2SO_4 that were consistent with gas-phase observations in the RMBL. Briefly, the DMS oxidation scheme is initialized by reactions with OH and NO_3, where the former occurs through two independent branches and the latter is potentially important at night. Initialization by halogens (e.g. von Glasow et al., 2002) is neglected here due to poorly-constrained reactive halogen concentrations in the RMBL. Overall, OH oxidation dominates the net photochemical loss of DMS in the RMBL because of the relatively abundant OH levels and large OH-related rate constants. As previously mentioned, OH oxidizes DMS through two channels, H-abstraction and OH-addition. The H-abstraction branch is favored at higher temperatures and primarily leads to SO_2 and H_2SO_4. The OH-addition branch has a negative temperature-dependence and leads to DMSO, $DMSO_2$, MSEA, and MSIA. The production of MSA is highly uncertain and is believed to form through both the H-abstraction and OH-addition channels. In this model, MSA is explicitly produced through the H-abstraction branch by reactions with CH_3SO_3. Through the OH-addition branch, however, MSA production is parameterized using first-order conversions from MSEA and MSIA using assumed rate constants derived from Lucas and Prinn (2002). Other notable reactions in the scheme include the isomerization of $CH_3S(O)_xOO$ to $CH_3S(O)_{x+2}$ and the temperature-dependent addition of O_2 to $CH_3S(O)_x$. Because NO_x levels are relatively low in the RMBL, the main oxidants in the mechanism are HO_x and O_3. Rather than predicting these oxidants directly in our model, we use measurement-based values to enable a specific focus on the sulfur-based chemistry.

ACPD
4, 6379–6430, 2004

2.1.2. Heterogeneous removal

Heterogeneous removal is formally estimated using $p_h = p_a + p_d$, where p_a and p_d are loss frequencies due to scavenging by aerosols and dry deposition at the ocean surface, respectively. Scavenging by aerosols dominates the net heterogeneous removal for most of the DMS oxidation products (i.e. $p_h \approx p_a$). For SO_2, however, both losses are important. The aerosol loss frequencies (p_a) are averages over the boundary layer portions of the observationally-based vertical scavenging profiles in Lucas and Prinn (2002), while the dry deposition losses (p_d) are set using typical dry deposition velocities for a stable RMBL. The p_h for SO_2 is taken as the empirically-derived removal frequency noted in Lucas and Prinn (2002). The net p_h values are listed in Table 1.

2.1.3. RMBL mixing

The first-order mixing coefficient (p_m) is based on the scaling $\partial/\partial z(K_z \partial n/\partial z) \sim p_m \Delta n$, which gives $p_m \sim K_z/(\Delta z)^2$, where K_z and Δz represent the vertical eddy-diffusion coefficient and mixing depth, respectively. This parameterization is applied to all of the important relatively long-lived DMS-related species, but not to the fast-reacting sulfur-based radicals. The specific value of $p_m = 4 \times 10^{-5}$ s^{-1} is estimated from $K_z \approx 10^5$ cm^2 s^{-1} and $\Delta z \approx 500$ m, which are typical values for a stable boundary layer in the remote marine atmosphere. The parameterized mixing scheme also requires the specification of the concentrations of relatively long-lived DMS-related species in the free troposphere (i.e. n_f). For simplicity and consistency, the n_f are fixed in time and based on the daily average "buffer layer" concentrations calculated in Lucas and Prinn (2002). The n_f values are given in Table 2.

2.1.4. DMS emissions

DMS emissions are usually calculated using the surface wind speed and the DMS concentrations in the air and sea. For the sake of simplicity, however, we assume a

ACPD
4, 6379–6430, 2004

constant oceanic emission rate of p_e = 9.5 × 10^4 molecules cm^{-3} s^{-1}. This emission rate is based on a previous estimate in the RMBL (Lucas and Prinn, 2002). For a mixed layer depth of 500 m, the corresponding DMS surface flux is comparable to the flux values of Bates et al. (1998b), Mari et al. (1999), and Shon et al. (2001).

2.2. Background conditions in the RMBL

The background meteorological and oxidizing conditions are defined using averages over the boundary layer in the model of Lucas and Prinn (2002). These conditions are originally based on the observations from Flight 24 of the First Aerosol Characterization Experiment (ACE-1) campaign (Bates et al., 1998a). Briefly, the flight occurred in the clear-sky over the Pacific Ocean near Tasmania. Five-day back trajectories indicated that the surface air masses were of a remote marine origin, and the region was characterized by relatively high DMS concentrations. The important oxidizing-related species OH, O_3, H_2O_2, and CH_3OOH were directly measured, which we use to drive the DMS model. Depending on their variations with time, the measurements were either time averaged or fit to time-dependent 'forcing' functions. The results are summarized in Table 2. Other important oxidants were either below the instrument detection limit (NO), or not measured (NO_2, NO_3, HO_2, and CH_3O_2). Given their importance in DMS oxidation, these species are diagnosed using the measured species or assumed as noted in Table 2.

2.3. Sources and treatment of uncertainties

A parametric, rather than a structural, analysis is our focus, so the model parameters are the only sources of uncertainty considered. The parameters are treated as random variables following lognormal probability distribution functions (PDFs). Table 1 lists the mean values ($\bar{p}$) and uncertainties (ϕ) of the parameters, where the uncertainties are specified as multiplicative factors (i.e. $\bar{p} \times \phi$ and $\bar{p} \times 1/\phi$). Lognormal parameter PDFs are used because they provide positive definite samples, thus preventing non-

ACPD
4, 6379–6430, 2004

physical negative values from entering the model. The uncertainty factor values are either derived from DeMore et al. (1997) and Atkinson et al. (1997) or have been set as in Lucas and Prinn (2002). When uncertainty information was not available, factors of 2.5 were generously assigned. Note that a factor of two uncertainty is generally prescribed for DMS emissions, which is smaller than the factor of 2.5 assumed here. Following DeMore et al. (1997) and Atkinson et al. (1997), the uncertainty factors are expressed by

$$\phi(T) = \phi_{298} \exp\left(\varepsilon \left| \frac{1}{T} - \frac{1}{298} \right| \right), \quad (2)$$

where ϕ_{298} is the value at 298 K and ε is used to the extrapolate to temperatures away from 298 K. The rate constants with $\varepsilon \neq 0$ impart a temperature-dependence to the uncertainties that are analyzed later on. For the SO_2+OH reaction, DeMore et al. (1997) list 4 separate sources of uncertainty that effect the overall rate constant parameter. We calculate the resulting 16 combinations, then estimate the overall uncertainty as $\log \phi \approx (\log p^+ - \log p^-)/2$, where p^+ and p^- are the maximum and minimum values, respectively.

Finally, note that the sensitivities and uncertainties are analyzed in logarithmic space using

$$\eta = \log n \quad \text{and} \quad \varrho = \log p, \quad (3)$$

where η and ϱ are the log-scaled concentrations (n) and parameters (p), respectively. Hereafter, the terms concentrations and parameters are used inter-changeably with logarithmic concentrations and parameters, though the specific context is apparent by the above notation.

3. Analytical methods

Two different methods are used in the sensitivity and uncertainty analysis. The first, referred to as the Direct Integration Method (DIM), directly integrates the concentration

ACPD
4, 6379–6430, 2004

and sensitivity ODEs. The second approach uses the Probabilistic Collocation Method (PCM) to generate a set of polynomial expansions that numerically approximate the solutions of the concentration ODEs.

3.1. Direct integration method

The direct integration method (e.g. Dickinson and Gelinas, 1976) integrates the ODEs in Eq. (1) and, optionally, the first-order sensitivity ODEs described in a following section (see Eq. 6). We use the stiff ODESSA solver from Leis and Kramer (1988a,b) for these direct integrations. ODESSA combines the decoupled direct algorithm (Dunker, 1984) with the standard LSODE solver (Hindmarsh and Radhakrishnan, 1993) to achieve efficient and reliable solutions for the concentrations and their sensitivities. There are no constraints on the output times using DIM, so it provides near-continuous solutions with time. Also, the sensitivities computed by DIM provide a basis for extrapolating concentration uncertainties. For practical reasons, however, DIM is limited to low-order sensitivity analyses.

3.2. Probabilistic collocation method

The solutions of the concentration ODEs are also estimated using the probabilistic collocation method. PCM, which is detailed in Tatang et al. (1997), has been applied to analyses of highly non-linear models of direct and indirect aerosol radiative forcing (Pan et al., 1997, 1998), and has been used to create parameterizations of non-linear chemical processing in an urban-scale model (Calbó et al., 1998; Mayer et al., 2000). Briefly, PCM estimates the model outputs as expansions of orthogonal polynomials of the model inputs. If the model inputs are cast as random variables, where each input parameter is defined by a PDF, the model output expansions become polynomial chaos expansions (PCEs) fit to the model output surface and weighting the high probability regions of the model inputs. The orthogonal polynomials are generated by recursive relationships based on the PDFs of the model inputs. The coefficients of the PCEs

ACPD
4, 6379–6430, 2004

are determined from multiple model runs at the collocation points of the input parameters. The DEMMUCOM package (Tatang, 1995) was used to determine the collocation points, construct the orthogonal polynomials, and perform the numerical fits.

3.2.1. Apply PCM to the DMS model

The inputs are the 56 uncertain model parameters listed in Table 1 and the outputs are the DMS-related concentrations. There is a trade-off between higher-order PCEs that capture model non-linearities, and lower-order PCEs that have a reasonable number of coefficients. For example, a full 3rd-order expansion for 56 inputs has 32 509 coefficients, while a full 2nd-order expansion has only 1653. As a compromise, the PCEs calculated here include homogeneous (pure) terms up to cubic order and all possible 2nd-order heterogeneous (cross) terms, resulting in expansions with 1709 coefficients. Separate PCEs were generated for the DMS-related species. Each PCE is given by ($M = 56$)

$$\hat{\eta} = \alpha_0 + \sum_{j=1}^{3}\sum_{k=1}^{M} \alpha_{j,k}\, g_{j,k}(\xi_k) + \sum_{k=1}^{M-1}\sum_{\ell=k+1}^{M} \beta_{k,\ell}\, g_{1,k}(\xi_k)\, g_{1,\ell}(\xi_\ell) \tag{4}$$

where $\hat{\eta}$ approximates the log-scaled concentration (i.e. $\hat{\eta} \approx \eta$), α_0 is the zeroth-order coefficient, $\alpha_{j,k}$ is the j-th order coefficient of the k-th parameter, $\beta_{k,\ell}$ is the coefficient of the 2nd-order cross term between input parameters k and ℓ, and $g_{j,k}(\xi_k)$ is the j-th order orthogonal polynomial for input parameter ξ_k (defined below). The coefficients in Eq. (4) are computed from 1709 runs using DIM at the set of input parameter collocation points. We fit to log-scaled concentrations above for two reasons. First, the solutions to chemical ODEs involve exponential functions, so log-scaling removes much of the exponential behavior and allows for better fits with lower-order polynomials. Second, lognormally distributed random variables naturally result from products of random variables, which are represented by the higher-order terms in the PCEs. Also, note that the PCEs are independent of time. They could be re-formulated to in-

ACPD
4, 6379–6430, 2004

clude a 'time' input having a uniform PDF. The resulting PCEs, however, would require much higher-order terms due to the large diurnal variations in DMS chemistry. In this sense, therefore, the nearly continuous solutions from DIM are an advantage over the time-discrete expansions from PCM.

3.2.2. Polynomial chaos expansions in ξ-space

The orthogonal polynomials $g_{j,k}(\xi_k)$ in Eq. (4) are expressed using standard normal random variables ξ_k. The random model parameters are transformed to standard normal random variables using $\varrho_k = \bar{\varrho}_k + \sigma_k \, \xi_k$, where ϱ_k is the k-th model parameter, and $\bar{\varrho}_k$ and σ_k are its mean value and standard deviation. This transformation yields a common set of orthogonal polynomials, shown in Table 3, that is used for all of the model parameters. Note that ξ_k defines the number of standard deviations ϱ_k lies from its mean value, where $\xi_k = 0$ is at the parameter mean and $|\xi_k| = 1$ is one standard deviation from the mean. This interpretation allows for the analysis of complex system behavior in a compact way and is used later on to describe uncertainty-dependent concentration sensitivities.

4. Sensitivity analysis

The sensitivity analysis considers the changes to the sulfur-based concentrations for infinitesimal changes in the model parameters. Three types of sensitivity coefficients are calculated: (1) time-dependent first-order; (2) uncertainty-dependent first-order; and (3) higher-order.

ACPD
4, 6379–6430, 2004

4.1. Time-dependent first-order sensitivities

The first-order sensitivity of concentration n_i to model parameter p_j is expressed as

$$z_{ij} = \frac{\partial n_i}{\partial p_j}. \tag{5}$$

Using this definition, the derivative of Eq. (1) with respect to parameter p_j leads to the following time-dependent system of concentration sensitivity ODEs

$$\frac{dz_{ij}}{dt} = \frac{\partial \dot{n}_i}{\partial p_j} + \sum_{k=1}^{N} \left(\frac{\partial \dot{n}_i}{\partial n_k} z_{kj} \right), \tag{6}$$

where $\dot{n}$ is the right hand side of Eq. (1). For N species and M parameters, Eqs. (1) and (6) form an $N \times (1 + M)$ coupled ODE system (i.e. 1425 ODEs for our DMS chemistry model). These equations are solved jointly using DIM. Moreover, because our model parameters have different units, we apply the following normalization

$$\frac{\partial \eta_i}{\partial \varrho_j} = \frac{\partial \log n_i}{\partial \log p_j} = \frac{p_j}{n_i} z_{ij}, \tag{7}$$

using the log-scaled concentrations and parameters. The normalized sensitivities are unitless and describe the fractional changes to the concentrations for fractional changes to the parameters. Note that higher-order sensitivities can be obtained by further differentiation of Eq. (6) with respect to the model parameters. The resulting system for the concentrations and the 1st- and 2nd-order sensitivity coefficients, however, yields $N \times (1 + M) \times (1 + M/2)$ ODEs (i.e. 41 325 in our DMS model). Thus, higher-order sensitivities are not calculated using DIM and are not typically analyzed in atmospheric chemistry models.

ACPD
4, 6379–6430, 2004

4.2. Uncertainty-dependent and higher-order sensitivities

The concentration sensitivities calculated by Eq. (6) do not account for uncertainties in the parameters. Our DMS model, however, has many highly uncertain parameters, which may yield concentration sensitivities that vary in magnitude and relative importance at parameter values away from their means. DIM can, in theory, calculate such uncertainty-dependent sensitivities by repeatedly solving Eqs. (1) and (6) using a Monte Carlo method on random samples from the parameter PDFs. This is not practical, however, given the 10^3 ODEs that need to be solved hundreds to thousands of times. PCM, on the other hand, is an efficient and powerful, albeit approximate, tool for calculating uncertainty-dependent sensitivities.

By taking the partial derivative of Eq. (4) with respect to model parameter ϱ_q we arrive at the following PCM-based estimate of the first-order concentration sensitivity

$$\frac{\partial \hat{\eta}}{\partial \varrho_q} = \frac{1}{\sigma_q} \left(\sum_{j=1}^{3} j \alpha_{j,q} g_{j-1,q}(\xi_q) + \sum_{\substack{k=1 \\ k \neq q}}^{M} \beta_{k,q} g_{1,k}(\xi_k) \right), \tag{8}$$

where σ_q is the standard deviation of ϱ_q. The uncertainty-dependence is exhibited by the ξ's on the right hand side of the equation. Note that the sensitivity of $\hat{\eta}$ to ϱ_q is a function of uncertainties in ϱ_q and ϱ_k. We evaluate this expression for $|\xi| \leq 1$. Furthermore, we compare this expression to the DIM-based first-order sensitivities in Eq. (6) by setting $\xi = 0$ above.

As noted before, higher-order concentration sensitivities are typically expensive to compute. Using PCM, however, they are easily generated by further differentiation of Eq. (8). Doing so, we derive the following second- and third-order sensitivity coefficients

$$\frac{\partial^2 \hat{\eta}}{\partial \varrho_q \partial \varrho_r} = \begin{cases} (2\,\alpha_{2,q} + 6\,\alpha_{3,q}\,g_{1,q}(\xi_q))/\sigma_q^2 & (q = r) \\ \beta_{q,r}/(\sigma_q \sigma_r) & (q \neq r) \end{cases} \tag{9}$$

ACPD
4, 6379–6430, 2004

$$\frac{\partial^3 \hat{\eta}}{\partial \varrho_q^3} = \frac{6\,\alpha_{3,q}}{\sigma_q^3}.$$

Note that only the homogeneous second-order sensitivities ($q = r$) are functions of ξ. Although these higher-order sensitivities are generally smaller than the first-order sensitivities, they can provide insight into couplings between model processes and other non-linearities. Thus, we compute and summarize the largest second- and third-order sensitivities.

5. Uncertainty analysis

The uncertainty analysis characterizes the uncertainties in the sulfur-based concentrations due to uncertainties in the model parameters. There are three stages in this analysis: (1) generate concentration PDFs and compute their first three moments; (2) calculate parameter contributions to the variance; and (3) analyze the net concentration uncertainties over a range of temperatures.

5.1. Probability density functions

Using a Monte Carlo method, we generate two different sets of concentration PDFs by drawing random samples from the parameter PDFs. The two sets are from separate multiple evaluations of Eq. (1) (labeled DIM-M) and Eq. (4) (labeled PCM). Computationally, the PDFs from PCM are less expensive because evaluating polynomials is more efficient than solving ODEs.

We also calculate the first three moments of the concentration PDFs. Using expected values, they are, respectively, $\langle\eta\rangle = E[\eta]$, $\sigma_\eta^2 = E[(\eta - \langle\eta\rangle)^2]$, and $\gamma_\eta = E[(\eta - \langle\eta\rangle)^3]/\sigma_\eta^3$, where $\langle\eta\rangle$ is the mean value, σ_η^2 is the variance, and γ_η is the skewness. Three different methods are used to estimate these moments: (1, DIM-S) the first-order sensitivities in Eq. (6) are projected to the concentration uncertainties from a single model run;

ACPD
4, 6379–6430, 2004

(2, DIM-M) standard expressions are directly evaluated for the DIM-M generated PDFs; and (3, PCM) we take the expected values of Eq. (4).

5.1.1. First moment

The DIM-S concentration mean values are estimated by

$$\langle \eta \rangle \approx \eta(\bar{\varrho}), \tag{10}$$

where $\eta(\bar{\varrho})$ is the value of η obtained from running the model at the parameter means. The concentration means are not strictly equal to the model evaluated at the parameter means (i.e. $\langle \eta \rangle \neq \eta(\bar{\varrho})$) because of higher-order terms. We truncate after the first term because the higher-order terms are typically negligible.

The DIM-M concentration mean values are estimated by

$$\langle \eta \rangle = \frac{1}{S} \sum_{j=1}^{S} \eta_j, \tag{11}$$

where η_j is the concentration value in each realization of Eq. (1) for a Monte Carlo sample size of S (we use $S = 10^4$).

The PCM moments are obtained by taking the expected value of Eq. (4). For independent random variables x and y, and constant a, the following properties are used: $E[x + y] = E[x] + E[y]$, $E[ax] = aE[x]$ and $E[xy] = E[x]E[y]$. Using these properties, along with the values in Table 3, the PCM concentration mean value is

$$\langle \hat{\eta} \rangle = \alpha_0. \tag{12}$$

Thus, the leading coefficients of the PCEs are the mean concentrations. Also note that setting $\xi = 0$ in Eq. (4) gives $\alpha_0 - \sum_k \alpha_{2,k}$. This shows, again, a difference between the concentration means and the concentrations at the parameter means.

ACPD
4, 6379–6430, 2004

5.1.2. Second moment

The DIM-S variances are estimated using

$$\sigma_\eta^2 \approx \sum_{j=1}^{M} \left(\frac{\partial \eta}{\partial \varrho_j} \right)^2 \sigma_j^2. \tag{13}$$

As before, we retain only the leading term because the higher-order terms are typically negligible. The truncated expression estimates the concentration uncertainties using only first-order sensitivity coefficients and parameter uncertainties. Note the summation over model parameters, which we later use to estimate the individual parameter contributions to the variance.

The DIM-M variances are estimated using

$$\sigma_\eta^2 = \frac{1}{S} \sum_{j=1}^{S} \left(\eta_j - \langle \eta \rangle \right)^2, \tag{14}$$

where $\langle \eta \rangle$ is from Eq. (11), and η_j is the concentration from each realization of Eq. (1) over a sample size S.

The PCM-based variance is derived from the expected value of $(\hat{\eta} - \alpha_0)^2$. Using the properties of expected values and Table 3, it is easy to show that the variance of Eq. (4) is

$$\sigma_{\hat{\eta}}^2 = \sum_{j=1}^{M} \left(\alpha_{1,j}^2 + 2\alpha_{2,j}^2 + 6\alpha_{3,j}^2 \right) + \sum_{j=1}^{M-1} \sum_{k=j+1}^{M} \beta_{j,k}^2. \tag{15}$$

The summations are over individual parameters and parameter pairs, which we use as an alternate methodology for analyzing variance contributions.

ACPD
4, 6379–6430, 2004

5.1.3. Third moment

The skewnesses of the DIM-M PDFs are estimated directly using

$$\gamma_\eta = \frac{1}{S\sigma_\eta^3} \sum_{j=1}^{S} \left(\eta_j - \langle\eta\rangle\right)^3, \tag{16}$$

for a Monte Carlo sample size of S.

The PCM-based skewness is obtained from the expected value of $(\hat{\eta} - \alpha_0)^3$, which results in

$$\gamma_{\hat{\eta}} = \frac{1}{\sigma_{\hat{\eta}}^3} \left\{ \sum_{j=1}^{M} \alpha_{2,j} \left[3\alpha_{1,j}^2 + 8\alpha_{2,j}^2 + 3\left(\alpha_{1,j} + 6\alpha_{3,j}\right)^2 \right] \right.$$
$$\left. +6 \sum_{j=1}^{M-1} \sum_{k=j+1}^{M} \left[\beta_{j,k}\alpha_{1,j}\alpha_{1,k} + \beta_{j,k}^2 \left(\alpha_{2,j} + \alpha_{2,k}\right) \right] +6 \sum_{j=1}^{M-2} \sum_{k=j+1}^{M-1} \sum_{\ell=k+1}^{M} \beta_{j,k}\beta_{j,\ell}\beta_{k,\ell} \right\}. \tag{17}$$

This expression potentially can be used to quantify parameter contributions to the total skewness, but this analysis is not carried out here.

5.2. Uncertainty contributions

The contributions of the uncertain model parameters to the net concentration variances are also calculated. This analysis allows for a potential reduction of model error by gaining better knowledge about a subset of the model parameters rather than blindly trying to improve the full parameter set. Of our three separate variance estimates, DIM-S and PCM (i.e. Eqs. 13 and 15) have explicit summations over model parameters. From Eq. (13), the DIM-S variance contribution of parameter j is $(\partial\eta/\partial\varrho_j)^2\sigma_j^2/\sigma_\eta^2$. From Eq. (15), the PCM variance contribution is $(\alpha_{1,j}^2 + 2\alpha_{2,j}^2 + 6\alpha_{3,j}^2 + \beta_{j,k}^2)/\sigma_{\hat{\eta}}^2$, which includes a contribution from the pair of model parameters j and k. Thus, PCM is useful

ACPD
4, 6379–6430, 2004

for evaluating the effects of uncertain coupled processes on the overall concentration uncertainties.

5.3. Uncertainty dependence on temperature

Temperature affects the DMS-related concentration uncertainties in two distinct ways. First, many of the rate constants in Table 1 are exponential functions of temperature, which causes reaction rates that vary strongly with temperature. For instance, the DMS+OH oxidation rate changes considerably as temperature increases from low values, where OH-addition is favored, to higher values, where H-abstraction is dominant. At low temperatures, therefore, the sulfur-based concentration uncertainties are less likely to have contributions from the uncertain DMS+OH abstraction rate constant. Second, many of the parameter uncertainties are also explicit functions of temperature (i.e. see Eq. 2) because the photochemical rate constants are most certain at room temperature and less certain at other temperatures. These two temperature-uncertainty effects may offset at one temperature and reinforce at another, because a particular reaction rate may decrease with falling temperature while its uncertainty increases. The DMS+OH abstraction reaction is a prime example, because the reaction rate decreases as temperature falls from 298 K, while the uncertainty in the rate constant increases. These two effects lead to possible non-linearities in the temperature-dependence of the concentration uncertainties. These potential non-linear temperature effects are diagnosed by calculating the sulfur-based concentrations (Eq. 1) and concentration uncertainties (Eqs. 6 and 13) over a temperature range of 250–310 K, preserving all of the other conditions in Table 2.

6. Results and discussion

The model is integrated until a repetitive diurnal cycle is achieved for all of the gas-phase DMS-related species. The following analysis is for the final day of this integra-

ACPD
4, 6379–6430, 2004

tion. Recall that PCM is limited to discrete times. PCEs, therefore, are constructed at local times (LT) 12:00 and 18:00 to provide contrast between periods of active and relatively inactive photochemistry. We limit our focus here to the sensitivities and uncertainties of DMS, SO_2, MSA, and H_2SO_4. A similar analysis for other sulfur-containing species (e.g. DMSO and $DMSO_2$) is found in Lucas (2003).

6.1. Concentrations

6.1.1. Diurnal concentration cycles

The diurnal cycles for DMS, SO_2, MSA, and H_2SO_4 calculated using DIM are displayed in Fig. 2. The DMS and SO_2 cycles have noticeably small amplitudes because they are strongly influenced by non-photochemical processes (e.g. mixing into or out of the RMBL). The MSA and H_2SO_4 cycles, on the other hand, have large amplitudes because their sources are dominated by chemistry. The DMS and SO_2 cycles are also strongly anti-correlated. This anti-correlation has been both observed and modeled in the RMBL (Davis et al., 1999; Chen et al., 2000), and serves as primary evidence that SO_2 in the marine environment is photochemically produced from DMS oxidation. The phases of the DMS and SO_2 cycles in Fig. 2 agree with the modeled cycles by Davis et al. (1999) and Chen et al. (2000); in particular their maxima and minima occur at roughly the same times. Our diurnal amplitudes for DMS and SO_2, however, are smaller than in Davis et al. (1999) and Chen et al. (2000), due in part to differing strengths of the OH cycles (i.e. tropical versus extratropical conditions).

6.1.2. DIM-PCM concentration correlations

We test the quality of the PCEs by comparing the concentrations from DIM (Eq. 1) with those from PCM (Eq. 4) for common random samples from the parameter PDFs. Using sample sizes of 10^3, DIM-PCM concentration correlations at 12:00 LT and 18:00 LT are shown in Fig. 3. Also shown are the 1:1 lines, coefficients of determination (R^2), and

ACPD
4, 6379–6430, 2004

indices of agreement (d). As indicated in the figure, the DIM and PCM concentrations are highly correlated at both times (i.e. R^2 and d are greater than 0.9). These strong concentration correlations hold by two to four orders of magnitude. This suggests that, overall, the PCEs with up to third-order homogeneous terms and second-order cross terms sufficiently represent the true model concentrations at 12:00 LT and 18:00 LT.

6.1.3. Concentration PCEs

Truncated forms of the concentration PCEs for DMS, SO_2, MSA, and H_2SO_4 are shown in Table 4. The leading terms of the PCEs are the concentrations at the parameter means (i.e. $\xi = 0$). The signs of the PCE coefficients (+/−) indicate whether the concentrations increase (+) or decrease (−) for increases in the magnitude of the specified parameter away from its mean value. The signs of the non-linear PCE coefficients also signal whether the concentration PDFs generated from these PCEs will be skewed to the left (−) or right (+) of the mean. Even in their truncated forms, these PCEs indicate that non-linearities and parameter couplings play an important role in determining the concentrations. For instance, the concentration of SO_2 in ξ-space depends on non-linear combinations of heterogeneous removal (ξ_{53}), DMS emissions (ξ_{55}), and RMBL mixing (ξ_{56}). The subsequent PCM-based sensitivities and PDF moments are acquired by taking derivatives and expected values of these PCEs.

6.2. Sensitivities

6.2.1. Diurnal first-order sensitivity cycles

Figure 4 shows the diurnal cycles of the normalized, first-order sensitivity coefficients for DMS, SO_2, MSA, and H_2SO_4 derived from Eqs. (6) and (7). The majority of the sensitivity coefficients are extremely time-dependent, showing rapid changes near midday and some changes in sign. Though complex, these sensitivities have the following general features related to the type of model process (i.e. chemistry, heterogeneous loss,

ACPD
4, 6379–6430, 2004

DMS emissions, or RMBL mixing). (1) The sensitivities to chemical production and loss reactions are positive and negative, respectively, with magnitudes that tend to follow photochemical activity. (2) The sensitivities to heterogeneous loss are negative and have their smallest magnitudes between morning and noon when photochemistry dominates the concentration changes. (3) The sensitivities to DMS emissions are positive, but linear for DMS and cyclical for the other species. This occurs because a change in DMS emissions yields a proportional change in the DMS concentration, which then undergoes photochemical oxidation. (4) The sensitivity to the RMBL mixing coefficient depends on the magnitude and sign of $n_f - n$ in Eq. (1). This difference is negative for DMS, positive for SO_2, and varies for MSA, with magnitudes related to their production cycles in the RMBL and the direction of the transport flux.

On the basis of their magnitudes, sensitivity coefficients are typically ranked to identify the most important parameters affecting a model output. Because the sensitivities in Fig. 4 vary with time, the most important parameters also vary with time. For example, H_2SO_4 is nearly equally sensitive to parameters 1 and 24 during the day, but not during the early morning and late evening. Considering these time variations, we summarize the parameters that are very influential during some portion of the diurnal cycle for each of the four species as follows: (1) DMS is primarily sensitive to the parameters for oceanic emissions and RMBL mixing, and moderately sensitive to the DMS+OH abstraction rate constant. (2) SO_2 is markedly sensitive to the parameters related to DMS emissions, RMBL mixing, heterogeneous loss, and the DMS+OH abstraction rate constant. (3) MSA is mainly sensitive to the parameters for DMS emissions, RMBL mixing, heterogeneous loss, the rate constant for DMS+OH addition, and the rate constants associated with the formation of MSEA and its subsequent conversion to MSA. (4) H_2SO_4 is sensitive to many parameters, including those for DMS emissions, heterogeneous loss, and the rate constants for DMS+OH abstraction, the reaction between CH_3SCH_2OO and NO, reactions of CH_3SO with O_2 and O_3, and the isomerization of $CH_3S(O)OO$ to CH_3SO_3.

It is also important to note that none of the four species is appreciably sensitive to

ACPD
4, 6379–6430, 2004

the rate constant for the oxidation of DMS by NO_3, even at night, because the concentration of NO_3 is relatively low in the RMBL. Furthermore, SO_2 does not show any significant sensitivity to CH_3SO_2 dissociation even though this path directly forms SO_2. This finding contradicts Saltelli and Hjorth (1995), who found CH_3SO_2 dissociation to be a critical reaction for both SO_2 and H_2SO_4. This discrepancy occurs because non-photochemical processes tend to be the dominant sensitivities in our model, and these processes are not included in Saltelli and Hjorth (1995). Also, our DMS mechanism contains a relatively efficient non-CH_3SO_2 pathway for producing H_2SO_4.

A final notable feature in Fig. 4 is the number of key parameters influencing the four species. Specifically, DMS and SO_2 are sensitive to a few parameters, while MSA and H_2SO_4 are sensitive to many. This occurs because MSA and H_2SO_4 are formed by a variety of pathways. Consequently, discarding those pathways with relatively low sensitivities reduces the size of the DMS mechanism by only a moderate amount. For example, retaining only those parameters that have sensitivities within 50% of the largest sensitivity for each species reduces the original mechanism by less than half (from 56 to 34 parameters). Therefore, commonly-used parameterized DMS mechanisms (e.g. the 4 reaction schemes used in Chin et al., 1996; Gondwe et al., 2003), are not fully resolving the production of the DMS end products.

6.2.2. Comparison of first-order sensitivities

Before analyzing the uncertainty-dependent and higher-order sensitivities using PCM, we first compare the first-order sensitivities calculated separately using DIM (Eq. 6) and PCM ($\xi = 0$ in Eq. 8). This comparison is shown in Fig. 5, where, due to the numerous model parameters, only the largest sensitivities are displayed. As shown in the figure, the DIM and PCM sensitivity coefficients agree in sign and magnitude. The agreement even holds over time, as exemplified by the sensitivity of H_2SO_4 to the CH_3SCH_2OO+NO reaction rate constant (parameter 12), which is positive at 12:00 LT and negative at 18:00 LT. Though the overall agreement is excellent, there are some slight systematic differences. For instance, many of the H_2SO_4 concentration sensitiv-

ACPD
4, 6379–6430, 2004

ities using DIM are systematically higher than the corresponding PCM-based sensitivities. These systematic differences are not related to the PCE fits though, because the concentration correlations in Fig. 3 do not show any significant biases towards DIM or PCM. Rather, the differences are likely due to the first-order versus higher-order nature between DIM and PCM, respectively. Nevertheless, the generally good agreement in Fig. 5 supports the most important parameters identified in the previous section, and allows for a confident assessment of the uncertainty-dependent and higher-order sensitivities in the next section.

6.2.3. Uncertainty-dependent sensitivities

Equation (8) is used to calculate the first-order, uncertainty-dependent sensitivity coefficients. Because the expressions are 56-dimensional polynomials, we cannot display them directly. Setting all of the parameters to their mean values except for parameter q (i.e. $\xi_k = 0 \; \forall \; k \neq q$), however, results in 1D quadratic polynomials that are readily displayed. Figure 6 shows the magnitudes of these 1D polynomials at local noon as parameter q is varied within $|\xi_q| \leq 1$. To interpret these plots, an increase in the vertical scale denotes an increased sensitivity to the indicated parameter, and the vertical ordering from top to bottom rates the parameters from most to least influential. As shown, the magnitudes of many of the sensitivities change dramatically with ξ. Some of these changes are as large as, or even larger than, the diurnal changes shown in Fig. 4. The sensitivity of SO_2 to the heterogeneous loss parameter, for example, changes by about 0.15 with time over a day and 0.4 over the range $|\xi| < 1$. Figure 6 also shows that the ratings of the most influential model parameters clearly change with ξ. DMS, for instance, is most sensitive to the surface emission parameter for all values of ξ except near -1, where it is the second largest sensitivity. Other notable shifts in the ratings occur for the sensitivities of (1) SO_2 and H_2SO_4 to the DMS+OH abstraction rate constant, (2) H_2SO_4 to the DMS emission rate, (3) MSA and H_2SO_4 to the RMBL mixing coefficient, and (4) MSA to the DMS+OH addition and CH_3SO_3 dissociation rate constants. These shifts result in sulfur-based concentrations that tend to be relatively more

ACPD
4, 6379–6430, 2004

sensitive to the chemical parameters (i.e. parameters 1–47) at lower values of ξ.

6.2.4. Higher-order sensitivities

The magnitudes of the three largest second- and third-order sensitivity coefficients using Eq. (9) are displayed in Fig. 7. For reference, the first-order sensitivities from Eq. (8) are also shown. Note that the first-order sensitivities tend to be larger than the higher-order terms, indicating concentration PCEs that are mainly linear in the parameters. There are, however, many extremely large second- and third-order sensitivities, which illustrates the presence of significant non-linear parameter dependencies. In particular, SO_2 has higher-order sensitivity coefficients that rival its first-order sensitivities. Upon inspection, the most significant higher-order sensitivities are related to the RMBL mixing parameter, which emphasizes the important role that mixing plays in regulating the RMBL concentrations of the DMS-related species. Other conclusions from Fig. 7 are: (1) The combination of DMS emissions and RMBL mixing is important, especially for SO_2. (2) The second-order coupling between the DMS+OH oxidation rate constants with the RMBL mixing parameter influences DMS, SO_2, and MSA. (3) The oxidized sulfur-bearing species have higher-order dependencies on their heterogeneous removal parameters. (4) The second-order co-variation between the heterogeneous removal rate and RMBL mixing coefficient is significant in the late afternoon for SO_2. (5) In the late afternoon, MSA has a fairly large dependence on the interaction between the rate constants associated with MSEA formation and the RMBL mixing parameter.

6.3. Uncertainties

6.3.1. Concentration PDFs

The concentration PDFs for DMS, SO_2, MSA, and H_2SO_4 are shown in Fig. 8. Recall, two separate sets of PDFs were obtained using Monte Carlo analysis on Eq. (1) (DIMM) and Eq. (4) (PCM). Qualitatively from the PDF widths, the concentrations of DMS

ACPD
4, 6379–6430, 2004

and SO_2 are moderately uncertain, while the concentrations of MSA and H_2SO_4 are highly uncertain. With time, the most probable values for DMS and SO_2 do not vary, but for MSA and H_2SO_4 they shift from higher to lower concentrations between midday and the afternoon. These shifts are related to the amplitudes of the diurnal cycles in Fig. 2 relative to the concentration uncertainties. SO_2, for instance, has a larger uncertainty than diurnal amplitude, and so the PDFs for SO_2 nearly overlap in time. Also note that the overall widths and shapes of the PDFs are largely invariant with time. Moreover, the concentration PDFs are similar between the two methods, which provides confidence in the following assessment of the PDF moments.

6.3.2. Comparison of PDF moments

The moments of the log-scaled concentrations are listed in Table 5. The mean values from DIM-M and PCM agree nearly perfectly at the given precision, which implies that the leading coefficients of the PCEs (α_0) are excellent estimators of the mean values. Comparing these to the DIM-S values, however, shows that the neglected higher-order term in Eq. (10) leads to quantitative differences for H_2SO_4 at 18:00 LT and MSA at both times. Because the mean values are logarithmic, these apparently small differences are actually 20% to 30% differences in the concentrations. Thus, concentrations calculated using the mean values of the model parameters are not necessarily good estimates of the mean values of the concentrations. This notion is also supported by PCM (i.e. the leading coefficients in Table 4 versus the mean values in Table 5).

The three estimates of the net variances of the log-scaled concentrations are also listed in Table 5. On the basis of these variances, the concentrations of DMS, SO_2, MSA, and H_2SO_4 are uncertain (2-σ) by factors of approximately 5, 3, 10, and 10, respectively. As before, the estimates using DIM-M and PCM are similar with each other, but differ from the DIM-S variances because of the neglected higher-order term in Eq. (13). This shows that extrapolating uncertainties from first-order sensitivities alone can be potentially misleading. This has also been commented on by Saltelli (1999). Nonetheless, our DIM-S variances are still reasonably consistent with the other

ACPD
4, 6379–6430, 2004

estimates. This, in turn, allows us to use DIM-S to easily calculate variations in the concentration uncertainties with time and temperature, as shown in a following section.

The skewness values listed in Table 5 confirm that the SO_2 PDFs are skewed to the left of the mean while the remaining PDFs are skewed to the right. With time, the PDFs tend to be more skewed in the afternoon than at noon. Although the DIM-M and PCM skewnesses differ, differences less than about 0.1 are not significant. Thus, we can draw important conclusions about the relationship between PDF symmetries and non-linearities in the DMS chemistry model. From the central limit theorem, sums and products of independent random variables tend towards normal and lognormal distributions, respectively. The PDFs in Fig. 8, therefore, are merely convolutions of normal and lognormal distributions because the DMS-related species depend on sums and products of the random model parameters. In this regard, PCM is a powerful technique because the PCEs explicitly decompose the concentrations into sums and products of random variables. By examining the magnitudes of the PCE coefficients for the non-linear terms, one can predict beforehand whether the resulting concentration PDFs are likely to be asymmetric. Furthermore, the non-linear combinations leading to any PDF asymmetries are readily identified. For example, the magnitudes of the PCE coefficients for DMS listed in Table 4 indicate that the PDF asymmetry stems from non-linearities involving the DMS emission rate, while the strong asymmetries for SO_2 involve non-linear combinations of the parameters related to heterogeneous removal, DMS emissions, RMBL mixing, and the DMS+OH addition rate constant.

6.3.3. Variance contributions

The contributions of uncertain parameters to the concentration variances of DMS, SO_2, MSA, and H_2SO_4 are displayed in Fig. 9, including contributions from pairs of uncertain parameters. Together, Figs. 5 and 9 highlight an important distinction between sensitivity and uncertainty analyses. SO_2, for example, is highly sensitive to the DMS+OH abstraction rate constant, yet this parameter makes only a minor contribution to the uncertainty in SO_2.

ACPD
4, 6379–6430, 2004

Overall, the variance contributions using DIM-S and PCM are consistent with each other. They differ by less than 3% for DMS, 6% for MSA, 10% for H_2SO_4, and 15% for SO_2. Note, however, that some of the differences are systematic. For example, the variance contributions to H_2SO_4 from uncertain rate constants involving $CH_3S(O)OO$ (i.e. parameters 24, 25, and 45) are systematically higher in DIM-S than PCM. The PCM contributions tend to be lower because the net variance is also spread across pairs of parameters.

We conclude that the parameters identified as major contributors to the concentration variances are fairly robust, given the generally good agreement between DIM-S and PCM. Consequently, the concentration uncertainties can be reduced by targeting these parameters. From Fig. 9 it is clear that better constraints on DMS emissions (parameter 55) and heterogeneous removal (parameters 48–54) will go a long way towards reducing the overall DMS-related uncertainties. Other important conclusions from Fig. 9 include: (1) Uncertain DMS emissions contribute 80% of the uncertainty in DMS and at least 10% in the other species. (2) The well-known DMS+OH abstraction rate constant does not make significant variance contributions. (3) Uncertain heterogeneous removal parameters account for more than 50% of the uncertainty in SO_2. (4) MSA and H_2SO_4 have contributions from a multitude of parameters. (5) The rate constants for DMS+OH addition and the coversion of MSEA to MSA are important sources of uncertainty in MSA. (6) Rate constants for the reactions involving $CH_3S(O)OO$ are large sources of uncertainty for H_2SO_4.

Lastly, it is difficult to gauge in Fig. 9 the net variance contributions from chemical parameters (1–47) versus physical parameters (48–56). Table 6 shows the sums of these contributions. As noted, physical parameters account for nearly all of the uncertainty in DMS and SO_2. Chemical parameters, however, comprise 29–60% of the total uncertainty in MSA and H_2SO_4. To achieve significant reductions in the net uncertainties of the oxidized DMS products, therefore, will require a better understanding of many reactions in the DMS mechanism. Moreover, the contributions from pairs of uncertain parameters are summed and shown in Table 6. Pairs of parameters are

ACPD
4, 6379–6430, 2004

found to account for 7 to 8% of the net uncertainty in SO_2 and 12 to 20% in MSA and H_2SO_4. As a result, efforts to reduce the uncertainties in the DMS-related concentrations should also seek to gain a better understanding of the interactions between the various processes.

6.3.4. Variations with temperature

The time-temperature concentration contours are shown in the upper panel in Fig. 10. The maximum concentrations of DMS and SO_2 occur at the highest temperatures, MSA at the lowest temperatures, and H_2SO_4 at intermediate temperatures. These trends are related to the temperature-dependent chemistry. DMS concentrations fall with temperature, for instance, because the net rate of oxidation by OH decreases with temperature. SO_2 concentrations increase with temperature because the DMS+OH abstraction and CH_3SO_2 dissociation reactions both have rate constants that increase with temperature. MSA concentrations decrease with temperature because MSA is formed through the OH-addition branch. H_2SO_4 concentrations have a complex temperature behavior resulting from a combination of rate constants with opposing temperature dependencies (i.e. DMS+OH abstraction and CH_3SO_2 dissociation versus CH_3SO+O_2 addition). On the basis of the magnitudes of the concentration variations in Fig. 10, DMS and SO_2 are not very sensitive to temperature changes, while MSA and H_2SO_4 are fairly sensitive. Also, the concentrations are most sensitive to temperature near midday, because photochemistry is the only temperature-dependent process considered in our model. Overall, the sulfur-based concentrations change more rapidly with time than temperature.

The time-temperature concentration uncertainty contours are shown in the lower panel in Fig. 10. The DMS and SO_2 concentration uncertainties are rather small (factors of about 2.3 and 1.7, respectively) and have small temperature variations. The MSA and H_2SO_4 concentration uncertainties, on the other hand, are larger (up to factors of 4.1) and have extensive temperature variations. Also apparent is the complex non-linear dependence on temperature. As previously noted, this non-linearity stems

ACPD
4, 6379–6430, 2004

from two temperature-dependent sources (i.e. rate constants and parameter uncertainties) that can reinforce or cancel each other. The uncertainty maxima in Fig. 10 provide a means to assess the relative importance of these two sources. Temperature-dependent rate constants are most certain at room temperature (see Eq. 2), and so concentration uncertainties dominated by rate constant uncertainties should follow a similar trend. Fig. 10 shows, however, that only the midday DMS uncertainty – with maxima at high and low temperatures – exhibits this behavior. Moreover, H_2SO_4 is most uncertain near room temperature, where the rate constants are most certain. These results clearly show that the temperature-dependent rate constants, not the temperature-dependent uncertainty factors of the rate constants, dominate the temperature trends of the concentration uncertainties. Lastly, note that, the MSA and H_2SO_4 uncertainties do not maximize at noon when the photochemistry peaks, but in the afternoon. Heterogeneous removal is the prime reason for this feature because it is the largest sink in the afternoon when the concentrations are high and the photochemistry is weak.

7. Conclusions

The direct integration and probabilistic collocation methods identified the key parameters and sources of uncertainty in the diurnal DMS cycle in the remote marine boundary layer. The sulfur-bearing compounds are particularly sensitive to the parameters associated with DMS emissions, mixing with the free troposphere, heterogeneous removal, and the DMS+OH addition and abstraction reactions. MSA and H_2SO_4 are additionally sensitive to numerous rate constants, which emphasizes the limited capability of using highly-parameterized DMS mechanisms to compute these species. Moreover, many of the concentration sensitivities differ substantially as a function of the parameter uncertainties. After reducing the parameter values by one standard deviation from their mean, for example, we find that the sensitivities to chemical parameters become relatively more important. This shows that uncertainty-dependent sensitivity techniques,

ACPD
4, 6379–6430, 2004

as provided automatically by the probabilistic collocation method, are useful for identifying the key parameters in systems with complex, highly-uncertain chemistry, such as the DMS cycle.

For the uncertainty analysis, we computed the probability distribution functions of the sulfur-based compounds by propagating parameter uncertainties through our model. The second moments of these PDFs indicate that the concentrations of DMS, SO_2, MSA, and H_2SO_4 are uncertain by factors of roughly 2.2, 1.8, 3.0, and 3.0, respectively. Additionally, the third moments of these PDFs highlight the extent of non-linearities in the DMS model. SO_2, for instance, has a strongly-asymmetric PDF due to combinations of the parameters for heterogeneous scavenging, DMS emissions, RMBL mixing, and the DMS+OH addition rate constant.

The analysis also identifies the sources of uncertainty in the DMS-related compounds. Uncertainty contributions and sensitivities differ because the former, but not the latter, account for parameter uncertainties. For example, the relatively well known DMS+OH abstraction rate constant is an important sensitivity, but not a crucial uncertainty contribution. Overall, the uncertainties in the DMS emissions and heterogeneous scavenging parameters are the predominant contributors. For MSA and H_2SO_4, however, many individual uncertain rate constants also contribute at a 5% or higher level. Furthermore, uncertain rate constants collectively account for 29–60% of the net uncertainty in MSA and H_2SO_4. Contributions from pairs of uncertain parameters were also quantified, where they collectively account for 12–20% of the net variances in the concentrations of MSA and H_2SO_4. These results imply that a detailed understanding of many, simultaneous processes is required to effectively reduce the uncertainties in the oxidized DMS products.

Uncertainty variations are also analyzed between 250–310 K because our model contains temperature-dependent rate constants and rate constant uncertainties. The resulting concentration uncertainties largely follow the temperature-dependent branching in the DMS oxidation mechanism (e.g. DMS+OH addition versus abstraction). We conclude, therefore, that rate constants, rather than their uncertainty expressions, are

ACPD
4, 6379–6430, 2004

the main source of variations to the temperature-dependent uncertainties. Moreover, this analysis also shows that the concentration uncertainties for DMS and SO_2 remain nearly constant over the full temperature range, while those for MSA and H_2SO_4 vary by factors of 2 to 4.

Acknowledgements. This work was supported by NASA grant NAG5-12099 and the federal and industrial sponsors of the MIT Joint Program on the Science and Policy of Global Change.

References

Andreae, M. and Crutzen, P.: Atmospheric Aerosols: Biogeochemical Sources and Role in Atmospheric Chemistry, Science, 276, 1052–1058, 1997. 6381

Atkinson, R., Baulch, D. L., Cox, R. A., Hampson, R., Kerr, J. A., Rossi, M. J., and Troe, J.: Evaluated Kinetic and Photochemical Data for Atmospheric Chemistry: Supplement VI, J. Phys. Chem. Ref. Data, 26, 1329–1499, 1997. 6387

Bates, T. S., Lamb, B. K., Guenther, A., Dignon, J., and Stoiber, R. E.: Sulfur Emissions to the Atmosphere from Natural Sources, J. Atmos. Chem., 14, 315–337, 1992. 6380

Bates, T. S., Huebert, B., Gras, J., Griffiths, F., and Durkee, P.: The International Global Atmospheric Chemistry (IGAC) Project's First Aerosol Characterization Experiment (ACE-1): Overview, J. Geophys. Res., 103, 16,297–16,318, 1998a. 6386

Bates, T. S., Kapustin, V. N., Quinn, P. K., Covert, D. S., Coffman, D. J., Mari, C., Durkee, P. A., De Bruyn, W. J., and Saltzman, E. S.: Processes controlling the distribution of aerosol particles in the lower marine boundary layer during the First Aerosol Characterization Experiment (ACE 1), J. Geophys. Res., 103, 16,369–16,383, 1998b. 6386

Calbó, J., Pan, W., Webster, M., Prinn, R., and McRae, G.: Parameterization of Urban Sub-Grid Scale Processes in Global Atmospheric Chemistry Models, J. Geophys. Res., 103, 3437–3452, 1998. 6388

Campolongo, F., Saltelli, A., Jensen, N. R., Wilson, J., and Hjorth, J.: The Role of Multiphase Chemistry in the Oxidation of Dimethylsulphide (DMS). A Latitude Dependent Study, J. Atmos. Chem., 32, 327–356, 1999. 6382

Capaldo, K. P. and Pandis, S. N.: Dimethylsulfide Chemistry in the Remote Marine Atmosphere:

Evaluation and Sensitivity Analysis of Available Mechanisms, J. Geophys. Res., 102, 23,251–23,267, 1997. 6381, 6382

Charlson, R., Lovelock, J., Andreae, M., and Warren, S.: Oceanic Phytoplankton, Atmospheric Sulphur, Cloud Albedo, and Climate, Nature, 326, 655–661, 1987. 6381

Chen, G., Davis, D. D., Kasibhatla, P., Bandy, A. R., Thornton, D. C., Huebert, B. J., Clarke, A. D., and Blomquist, B. W.: A Study of DMS Oxidation in the Tropics: Comparison of Christmas Island Field Observations of DMS, SO_2, and DMSO with Model Simulations, J. Atmos. Chem., 37, 137–160, 2000. 6383, 6398

Chin, M., Jacob, D. J., Gardner, G. M., Foreman-Fowler, M. S., Spiro, P. A., and Savoie, D. L.: A Global Three-Dimensional Model of Tropospheric Sulfate, J. Geophys. Res., 101, 18,667–18,690, 1996. 6401

Davis, D., Chen, G., Bandy, A., Thornton, D., Eisele, F., Mauldin, L., Tanner, D., Lenschow, D., Fuelberg, H., Huebert, B., Heath, J., Clarke, A., and Blake, D.: Dimethyl Sulfide Oxidation in the Equatorial Pacific: Comparison of Model Simulations with Field Observations for DMS, SO_2, H_2SO_4(g), MSA(g), MS, and NSS, J. Geophys. Res., 104, 5765–5784, 1999. 6383, 6398

DeMore, W., Sander, S., Golden, D., Hampson, R., Howard, C., Ravishankara, A., Kolb, C., and Molina, M.: Chemical Kinetics and Photochemical Data for Use in Stratospheric Modeling, Tech. Rep. Evaluation No. 12, Jet Propulsion Laboratory, NASA, Pasadena, CA, 1997. 6387

Dickinson, R. P. and Gelinas, R. J.: Sensitivity Analysis of Ordinary Differential Equation Systems - A Direct Method, J. Comp. Phys., 21, 123–143, 1976. 6382, 6388

Dunker, A. M.: The Decoupled Direct Method for Calculating Sensitivity Coefficients in Chemical Kinetics, J. Chem. Phys., 81, 2385–2393, 1984. 6388

Gondwe, M., Krol, M., Gieskes, W., Klaassen, W., and de Baar, H.: The Contribution of Ocean-Leaving DMS to the Global Atmospheric Burdens of DMS, MSA, SO_2, and NSS $SO_4^=$, Global Biogeochem. Cycles, 17, 1056, doi:10.1029/2002GB001937, 2003. 6401

Hindmarsh, A. and Radhakrishnan, K.: Description and Use of LSODE, the Livermore Solver for Ordinary Differential Equations, Tech. Rep. UCRL-ID-113855, Lawrence Livermore National Laboratory, Livermore, CA, 1993. 6388

Keller, M., Bellows, W., and Guillard, R.: Dimethylsulfide Production in Marine Phytoplankton, in Biogenic Sulfur in the Environment, edited by E. Saltzman and W. Cooper, pp. 167–182, American Chemical Society, Washington, D.C., 1989. 6380

Kulmala, M., Laaksonen, A., and Pirjola, L.: Parameterizations for Sulfuric Acid/Water Nucle-

ACPD

4, 6379–6430, 2004

ation Rates, J. Geophys. Res., 103, 8301–8307, 1998. 6381
Leis, J. R. and Kramer, M. A.: The Simultaneous Solution and Sensitivity Analysis of Systems Described by Ordinary Differential Equations, ACM Trans. Math. Software, 14, 45–60, 1988a. 6382, 6388
Leis, J. R. and Kramer, M. A.: Algorithm 658: ODESSA - An Ordinary Differential Equation Solver With Explicit Simultaneous Sensitivity Analysis, ACM Trans. Math. Software, 14, 61–67, 1988b. 6388
Liss, P. S. and Merlivat, L.: Air-sea gas exchange rates: Introduction and synthesis, in The Role of Air-Sea Exchange in Geochemical Cycling, edited by P. Buat-Ménard and D. Reidel, pp. 113-127, Norwell, Mass, 1986. 6381
Lucas, D. D.: Mechanistic, Sensitivity, and Uncertainty Studies of the Atmospheric Oxidation of Dimethylsulfide, Ph.D. thesis, Massachusetts Institute of Technology, Cambridge, MA, Center for Global Change Science Report 71, http://web.mit.edu/cgcs/www/MIT_CGCS_Rpt71.html, 2003. 6383, 6398
Lucas, D. D. and Prinn, R. G.: Mechanistic Studies of Dimethylsulfide Oxidation Products Using an Observationally Constrained Model, J. Geophys. Res., 107, 4201, doi:10.1029/2001JD000843, 2002. 6381, 6383, 6384, 6385, 6386, 6387, 6414, 6416
Lucas, D. D. and Prinn, R. G.: Tropospheric distributions of sulfuric acid-water vapor aerosol nucleation rates from dimethylsulfide oxidation, Geophys. Res. Lett., 30, 2136, doi:10.1029/2003GL018370, 2003. 6383
Mari, C., Suhre, K., Rosset, R., Bates, T. S., Huebert, B. J., Bandy, A. R., Thorton, D. C., and Businger, S.: One-Dimensional Modeling of Sulfur Species During the First Aerosol Characterization Experiment (ACE 1) Lagrangian B, J. Geophys. Res., 104, 21,733–21,749, 1999. 6386
Mayer, M., Wang, C., Webster, M., and Prinn, R. G.: Linking Local Air Pollution to Global Chemistry and Climate, J. Geophys. Res., 105, 22,869–22,896, 2000. 6388
Pan, W., Tatang, M., McRae, G., and Prinn, R.: Uncertainty Analysis of Direct Radiative Forcing by Anthropogenic Sulfate Aerosols, J. Geophys. Res., 102, 21,915–21,924, 1997. 6388
Pan, W., Tatang, M., McRae, G., and Prinn, R.: Uncertainty Analysis of Indirect Radiative Forcing by Anthropogenic Sulfate Aerosols, J. Geophys. Res., 103, 3815–3824, 1998. 6388
Restelli, G. and Angeletti, G., eds.: Dimethylsulphide: Oceans, Atmosphere, and Climate, Kluwer, Dordrecht, Netherlands, 1993. 6381
Saltelli, A.: Sensitivity Analysis: Could Better Methods Be Used?, J. Geophys. Res., 104,

ACPD
4, 6379–6430, 2004

3789–3793, 1999. 6382, 6404
Saltelli, A. and Hjorth, J.: Uncertainty and Sensitivity Analyses of OH-Initiated Dimethyl Sulphide (DMS) Oxidation Kinetics, J. Atmos. Chem., 21, 187–221, 1995. 6382, 6401
Shaw, G.: Bio-Controlled Thermostasis Involving the Sulfur Cycle, Climatic Change, 5, 297–303, 1983. 6381
Shon, Z., Davis, D., Chen, G., Grodzinsky, G., Bandy, A., Thorton, D., Sandholm, S., Bradshaw, J., Stickel, R., Chameides, W., Kok, G., Russell, L., Mauldin, L., Tanner, D., and Eisele, F.: Evaluation of the DMS Flux and its Conversion to SO_2 over the Southern Ocean, Atmos. Environ., 35, 159–172, 2001. 6383, 6386
Tatang, M.: Direct Incorporation of Uncertainty in Chemical and Environmental Engineering Systems, Ph.D. thesis, MIT, Cambridge, MA, 1995. 6389
Tatang, M., Pan, W., Prinn, R., and McRae, G.: An Efficient Method for Parametric Uncertainty Analysis of Numerical Geophysical Models, J. Geophys. Res., 102, 21,925–21,932, 1997. 6382, 6388
Turnipseed, A. A. and Ravishankara, A. R.: The Atmospheric Oxidation of Dimethyl Sulfide: Elementary Steps in a Complex Mechanism, in Dimethylsulphide: Oceans, Atmospheres, and Climate, edited by G. Restelli and G. Angeletti, pp. 185–195, Kluwer, Dordrecht, 1993. 6381
Urbanski, S. P. and Wine, P. H.: Chemistry of Gas Phase Organic Sulfur-Centered Radicals, in S-Centered Radicals, edited by Z. B. Alfassi, pp. 97–140, Wiley, Chichester, 1999. 6381
Verheggen, B. and Mozurkewich, M.: Determination of Nucleation and Growth Rates from Observations of a SO_2 Induced Atmospheric Nucleation Event, J. Geophys. Res., 107, 4123, doi:10.1029/2001JD000683, 2002. 6381
von Glasow, R., Sander, R., Bott, A., and Crutzen, P. J.: Modeling Halogen Chemistry in the Marine Boudary Layer 2. Interactions With Sulfur and the Cloud-Covered MBL, J. Geophys. Res., 107, 4323, doi:10.1029/2001JD000943, 2002. 6384
Wanninkhof, R.: Relationship Between Wind Speed and Gas Exchange over the Ocean, J. Geophys. Res., 97, 7373–7382, 1992. 6381
Yin, F., Grosjean, D., and Seinfeld, J.: Photooxidation of Dimethyl Sulfide and Dimethyl Disulfide. I. Mechanism Development, J. Atmos. Chem., 11, 309–364, 1990. 6381

Table 1. Processes and parameters in the model of DMS chemistry in the remote marine boundary layer. The mean values of the parameters ($\bar{p}$) are listed as (p_0, p_T) and are calculated using $\bar{p}(T) = p_0 \exp(-p_T/T)$, where T is the temperature in degrees K. The parameter units are: first-order chemistry, s^{-1}; second-order chemistry, cm^3 $molecule^{-1}$ s^{-1}; heterogeneous loss, s^{-1}; DMS surface emission, molecules cm^{-3} s^{-1}; and RMBL mixing coefficient, s^{-1}. Uncertainties are listed as multiplicative factors using (ϕ_{298}, ε), where ϕ_{298} and ε are described in Eq. (2). Entries denoted by † are described in the text or in Lucas and Prinn (2002). Refer to Lucas and Prinn (2002) for further details.

Process		Mean Value	Uncertainty
Gas-Phase DMS Chemistry			
1	$CH_3SCH_3 + OH \rightarrow CH_3SCH_2 + H_2O$	(1.2E-11, 260)	(1.15, 100)
2	$CH_3SCH_3 + NO_3 \rightarrow CH_3SCH_2 + HNO_3$	(1.9E-13, -500)	(1.2, 200)
3	$CH_3SCH_3 + OH \rightarrow CH_3S(OH)CH_3$	†	(2.0, 0)
4	$CH_3S(OH)CH_3 \rightarrow CH_3SCH_3 + OH$	†	(2.5, 0)
5	$CH_3S(OH)CH_3 + O_2 \rightarrow CH_3S(O)CH_3 + HO_2$	(5.0E-13, 0)	(1.34, 0)
6	$CH_3S(OH)CH_3 \rightarrow CH_3SOH + CH_3$	(5.0E5, 0)	(2.5, 0)
7	$CH_3S(O)CH_3 + OH \rightarrow CH_3S(O)(OH)CH_3$	(6.3E-12, -800)	(1.3, 0)
8	$CH_3S(O)(OH)CH_3 + O_2 \rightarrow CH_3S(O)_2CH_3 + HO_2$	(1.0E-13, 0)	(2.5, 0)
9	$CH_3S(O)(OH)CH_3 \rightarrow CH_3S(O)OH + CH_3$	(2.0E6, 0)	(2.5, 0)
10	$CH_3S(O)OH + OH \rightarrow CH_3SO_2 + H_2O$	(1.0E-12, 0)	(2.5, 0)
11	$CH_3SCH_2 + O_2 \rightarrow CH_3SCH_2OO$	(5.7E-12, 0)	(1.07, 0)
12	$CH_3SCH_2OO + NO \rightarrow CH_3SCH_2O + NO_2$	(7.9E-12, -128)	(2.5, 0)
13	$CH_3SCH_2O \rightarrow CH_3S + CH_2O$	(3.3E4, 0)	(2.5, 0)
14	$CH_3SOH + OH \rightarrow CH_3SO + H_2O$	(5.0E-11, 0)	(2.5, 0)
15	$CH_3S + NO_2 \rightarrow CH_3SO + NO$	(2.1E-11, -320)	(1.15, 100)
16	$CH_3S + O_3 \rightarrow CH_3SO + O_2$	(2.0E-12, -290)	(1.15, 100)
17	$CH_3S + O_2 \rightarrow CH_3SOO$	(1.4E-16, -1550)	(2.0, 0)
18	$CH_3SOO \rightarrow CH_3S + O_2$	(1.5E11, 3910)	(2.0, 0)
19	$CH_3SOO + NO \rightarrow CH_3SO + NO_2$	(1.1E-11, 0)	(2.0, 100)
20	$CH_3SOO + NO_2 \rightarrow CH_3SOONO_2$	(2.2E-11, 0)	(2.0, 100)
21	$CH_3SOONO_2 \rightarrow CH_3SOO + NO_2$	(4.0E-3, 0)	(2.5, 0)
22	$CH_3SO + NO_2 \rightarrow CH_3SO_2 + NO$	(1.2E-11, 0)	(1.4, 0)

ACPD
4, 6379–6430, 2004

Table 1. Continued.

	Process	Mean Value	Uncertainty
	Gas-Phase DMS Chemistry		
23	$CH_3SO + O_3 \rightarrow CH_3SO_2 + O_2$	(6.0E-13, 0)	(1.5, 0)
24	$CH_3SO + O_2 \rightarrow CH_3S(O)OO$	(3.6E-16, -1550)	(2.5, 0)
25	$CH_3S(O)OO \rightarrow CH_3SO + O_2$	(3.9E11, 3910)	(2.5, 0)
26	$CH_3S(O)OO + NO \rightarrow CH_3SO_2 + NO_2$	(8E-12, 0)	(2.5, 0)
27	$CH_3S(O)OO + NO_2 \rightarrow CH_3S(O)OONO_2$	(1E-12, 0)	(2.5, 0)
28	$CH_3S(O)OONO_2 \rightarrow CH_3S(O)OO + NO_2$	(4.2E-3, 0)	(2.5, 0)
29	$CH_3SO_2 + NO_2 \rightarrow CH_3SO_3 + NO$	(2.2E-12, 0)	(1.5, 0)
30	$CH_3SO_2 + O_3 \rightarrow CH_3SO_3 + O_2$	(5.0E-15, 0)	(2.5, 0)
31	$CH_3SO_2 + OH \rightarrow CH_3SO_3H$	(5.0E-11, 0)	(2.5, 0)
32	$CH_3SO_2 + O_2 \rightarrow CH_3S(O)_2OO$	(1.2E-16, -1550)	(2.5, 0)
33	$CH_3S(O)_2OO \rightarrow CH_3SO_2 + O_2$	(1.3E11, 3910)	(2.5, 0)
34	$CH_3S(O)_2OO + NO \rightarrow CH_3SO_3 + NO_2$	(1.0E-11, 0)	(2.5, 0)
35	$CH_3S(O)_2OO + CH_3O_2 \rightarrow CH_3SO_3 + CH_2O + HO_2$	(5.5E-12, 0)	(2.5, 0)
36	$CH_3S(O)_2OO + NO_2 \rightarrow CH_3S(O)_2OONO_2$	(1.0E-12, 0)	(2.5, 0)
37	$CH_3S(O)_2OONO_2 \rightarrow CH_3S(O)_2OO + NO_2$	(4.2E-3, 0)	(2.5, 0)
38	$CH_3SO_2 \rightarrow CH_3 + SO_2$	†	(2.5, 0)
39	$CH_3SO_3 \rightarrow CH_3 + SO_3$	(1.6E-1, 0)	(2.5, 0)
40	$CH_3SO_3 + HO_2 \rightarrow CH_3SO_3H + O_2$	(5.0E-11, 0)	(2.5, 0)
41	$SO_2 + OH \rightarrow HOSO_2$	†	†
42	$HOSO_2 + O_2 \rightarrow SO_3 + HO_2$	(1.3E-12, 330)	(1.2, 200)
43	$SO_3 + H_2O \rightarrow H_2SO_4$	†	(2.0, 110)
44	$CH_3SOO \rightarrow CH_3SO_2$	(1.0, 0)	(2.5, 0)
45	$CH_3S(O)OO \rightarrow CH_3SO_3$	(0.08, 0)	(2.5, 0)
46	$CH_3S(O)OH \rightarrow CH_3SO_3H$	(1.0E-6, 0)	(2.5, 0)
47	$CH_3SOH \rightarrow CH_3SO_3H$	(5.0E-5, 0)	(2.5, 0)
	Non-Gas-Phase Processes		
48	$CH_3S(O)CH_3 \rightarrow$ heterogeneous loss	(2.0E-4, 0)	(2.2, 0)
49	$CH_3S(O)_2CH_3 \rightarrow$ heterogeneous loss	(2.0E-4, 0)	(2.2, 0)
50	$CH_3SOH \rightarrow$ heterogeneous loss	(5.0E-5, 0)	(2.5, 0)
51	$CH_3SO_2H \rightarrow$ heterogeneous loss	(5.0E-5, 0)	(2.5, 0)
52	$CH_3SO_3H \rightarrow$ heterogeneous loss	(2.0E-4, 0)	(2.2, 0)
53	$SO_2 \rightarrow$ heterogeneous loss	(5.0E-5, 0)	(2.5, 0)
54	$H_2SO_4 \rightarrow$ heterogeneous loss	(1.0E-3, 0)	(1.8, 0)
55	DMS surface emission	(9.5E4, 0)	(2.5, 0)
56	RMBL mixing coefficient	(4.0E-5, 0)	(1.5, 0)

ACPD

4, 6379–6430, 2004

Table 2. Background conditions in the model of DMS chemistry in the RMBL. Each condition is "fixed" or "varies" with time as noted in the right column. Diurnal time variations are expressed by $\Phi(a, b, c) = a \sin[\pi(t - 4.4)/15.2 + c] + b$, where t is the local time (hours from midnight), a is the amplitude (set to zero at night), b is the nighttime value, and c is the phase. The values of a and b are based on the fits to the ACE-1 Flight 24 observations. Units are explicitly given except for species in square brackets, which have concentration units of $\log_{10}$ (molecules cm^{-3}).

Condition	Value	Time
ACE-1 Flight 24		
mixed layer depth	500 m	fixed
temperature	290 K	fixed
pressure	990 hPa	fixed
relative humidity	75%	fixed
O_3	20 ppb	fixed
[OH]	$\Phi(1.7, 4.8, 0)$	varies
H_2O_2	$\Phi(0.40, 0.0068, 0)$ ppb	varies
CH_3OOH	$\Phi(0.20, 0.0034, 0)$ ppb	varies
Assumed		
NO	1 ppt	fixed
$[NO_3]$	$\Phi(2.0, 5.5, \pi)$	varies
Diagnosed		
HO_2	see Lucas and Prinn (2002)	varies
CH_3O_2	see Lucas and Prinn (2002)	varies
NO_2	see Lucas and Prinn (2002)	varies
Free Tropospheric Concentrations		
[DMS]	8.6	fixed
[DMSO]	6.8	fixed
$[DMSO_2]$	6.4	fixed
[MSEA]	6.6	fixed
[MSIA]	8.3	fixed
[MSA]	6.4	fixed
$[SO_2]$	9.1	fixed
$[H_2SO_4]$	6.6	fixed

ACPD
4, 6379–6430, 2004

Table 3. Orthogonal polynomials used in the polynomial chaos expansions. The orthogonal polynomials are in terms of standard normal random variable ξ. The first derivatives and expected values of the orthogonal polynomials are also given, where the expected values are calculated from $E[g_j^q] = \frac{1}{\sqrt{2\pi}} \int_{-\infty}^{\infty} \exp(-\xi^2/2)\, g_j^q(\xi)\, d\xi$.

Order	Polynomial	$\frac{\partial g_j}{\partial \xi}$	$E[g_j]$	$E[g_j^2]$	$E[g_j^3]$
0	$g_0 = 1$	0	1	1	1
1	$g_1 = \xi$	$1\, g_0$	0	1	0
2	$g_2 = \xi^2 - 1$	$2\, g_1$	0	2	8
3	$g_3 = \xi^3 - 3\,\xi$	$3\, g_2$	0	6	0
4	$g_4 = \xi^4 - 6\,\xi^2 + 3$	$4\, g_3$	0	24	1728

ACPD
4, 6379–6430, 2004

Table 4. Polynomial chaos expansions of the DMS-related species. The PCEs give the logarithmic concentrations ($\log_{10}$ molecules cm^{-3}) in terms of the standard normal random variables ξ_k, where k denotes the parameter number listed in Table 1. PCEs are ordered by the magnitudes of the coefficients and are truncated after the sixth largest coefficient.

Time	Species	Polynomial chaos expansion ($\log_{10}$ molecules cm^{-3})
12:00	DMS	$9.36 + 0.339\ \xi_{55} - 0.129\ \xi_{56} + 0.028\ \xi_{55}^2 - 0.020\ \xi_{55}\ \xi_{56} - 0.014\ \xi_3 + 0.010\ \xi_4 + \cdots$
	SO_2	$8.85 - 0.182\ \xi_{53} + 0.089\ \xi_{55} - 0.055\ \xi_{55}\ \xi_{56} + 0.041\ \xi_{56} - 0.036\ \xi_{53}^2 + 0.028\ \xi_{55}^2 + \cdots$
	MSA	$6.44 - 0.235\ \xi_{52} + 0.217\ \xi_{55} + 0.125\ \xi_{47} + 0.119\ \xi_6 + 0.110\ \xi_{40} + 0.100\ \xi_3 + \cdots$
	H_2SO_4	$6.82 - 0.236\ \xi_{54} + 0.207\ \xi_{55} - 0.170\ \xi_{25} + 0.139\ \xi_{45} + 0.139\ \xi_{24} - 0.087\ \xi_{53} + \cdots$
18:00	DMS	$9.36 + 0.339\ \xi_{55} - 0.116\ \xi_{56} + 0.028\ \xi_{55}^2 - 0.020\ \xi_{55}\ \xi_{56} - 0.013\ \xi_3 + 0.010\ \xi_4 + \cdots$
	SO_2	$8.85 - 0.228\ \xi_{53} + 0.077\ \xi_{55} + 0.046\ \xi_{53}\ \xi_{56} - 0.043\ \xi_{55}\ \xi_{56} - 0.042\ \xi_{53}^2 + 0.023\ \xi_{56} + \cdots$
	MSA	$6.29 - 0.347\ \xi_{52} + 0.160\ \xi_{55} + 0.116\ \xi_6 + 0.115\ \xi_{47} + 0.105\ \xi_3 + 0.092\ \xi_{46} + \cdots$
	H_2SO_4	$6.06 - 0.276\ \xi_{54} + 0.217\ \xi_{55} - 0.176\ \xi_{25} + 0.172\ \xi_{45} + 0.171\ \xi_{24} - 0.146\ \xi_{12} + \cdots$

ACPD
4, 6379–6430, 2004

Table 5. Moments of the DMS-related logarithmic concentration probability density functions ($\log_{10}$ molecules cm^{-3}). The DIM-M moments were calculated using a Monte Carlo sample size of 10^4.

Time	Species	Mean			Variance			Skewness	
		DIM-S	DIM-M	PCM	DIM-S	DIM-M	PCM	DIM-M	PCM
12:00	DMS	9.36	9.38	9.38	0.13	0.12	0.12	0.38	0.49
	SO_2	8.86	8.85	8.85	0.046	0.054	0.058	−0.61	−0.56
	MSA	6.43	6.55	6.53	0.23	0.22	0.26	0.35	0.48
	H_2SO_4	6.78	6.79	6.80	0.28	0.21	0.20	0.31	0.39
18:00	DMS	9.36	9.38	9.38	0.13	0.12	0.12	0.44	0.49
	SO_2	8.85	8.84	8.84	0.059	0.066	0.071	−0.64	−0.69
	MSA	6.27	6.36	6.36	0.22	0.22	0.24	0.41	0.48
	H_2SO_4	6.03	6.11	6.10	0.37	0.27	0.26	0.45	0.71

ACPD
4, 6379–6430, 2004

Table 6. Percent contributions to the concentration variances from chemical and physical parameters. The PCM values include variance contributions from pairs of uncertain parameters, including chemical-physical pairs listed under the "Cross" column.

Time	Species	Parameters				
		Chemical		Physical		Cross
		DIM-S	PCM	DIM-S	PCM	PCM
12:00	DMS	<1	<1	100	100	<1
	SO_2	3	4	97	95	8
	MSA	49	54	51	43	20
	H_2SO_4	55	41	45	54	12
18:00	DMS	<1	<1	100	100	<1
	SO_2	1	2	99	97	7
	MSA	33	29	67	64	14
	H_2SO_4	60	42	40	52	13

ACPD
4, 6379–6430, 2004

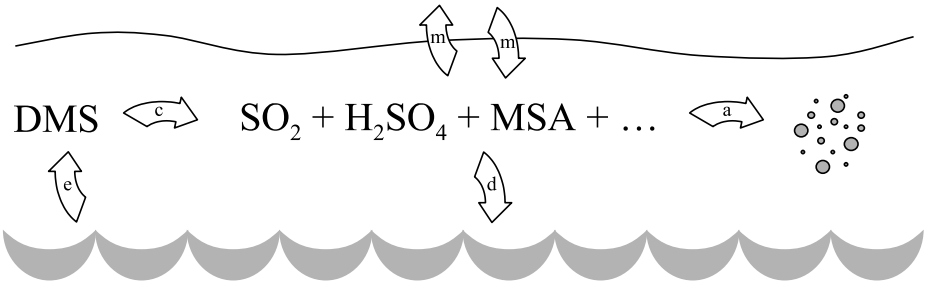

Fig. 1. Major processes affecting gas-phase DMS-related species in the RMBL: *e* = emissions of DMS from the ocean, *c* = chemical oxidation, *d* = dry deposition, *a* = loss to background aerosols, and *m* = mixing in to and out of the RMBL.

ACPD
4, 6379–6430, 2004

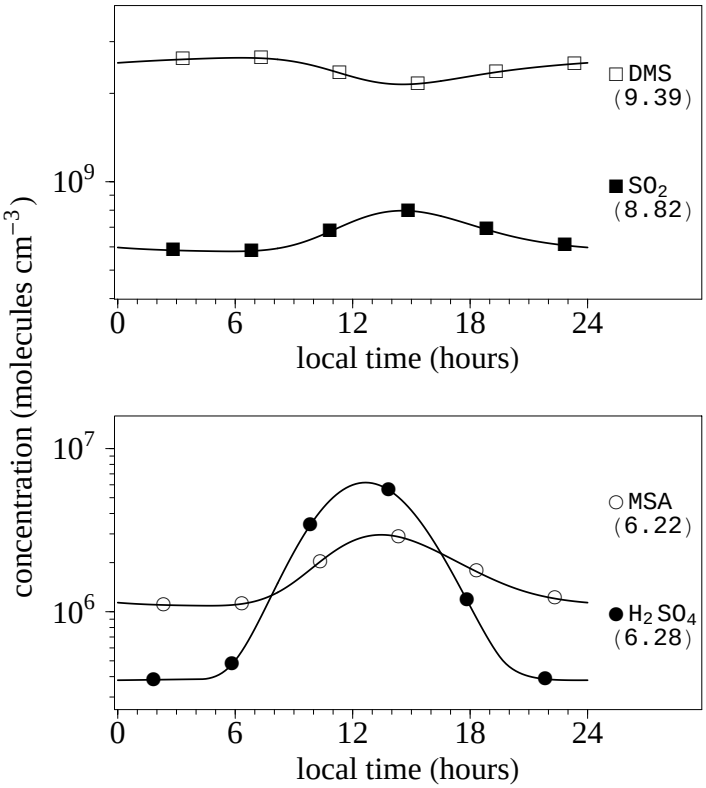

Fig. 2. Diurnal cycles of the concentrations (molecules cm^{-3}) of DMS, SO_2, MSA, and H_2SO_4. The labels on the individual profiles are given to the right and the daily average logarithmic concentrations are given in parentheses.

ACPD
4, 6379–6430, 2004

Sensitivities and uncertainties of DMS oxidation in the RMBL

D. D. Lucas and
R. G. Prinn

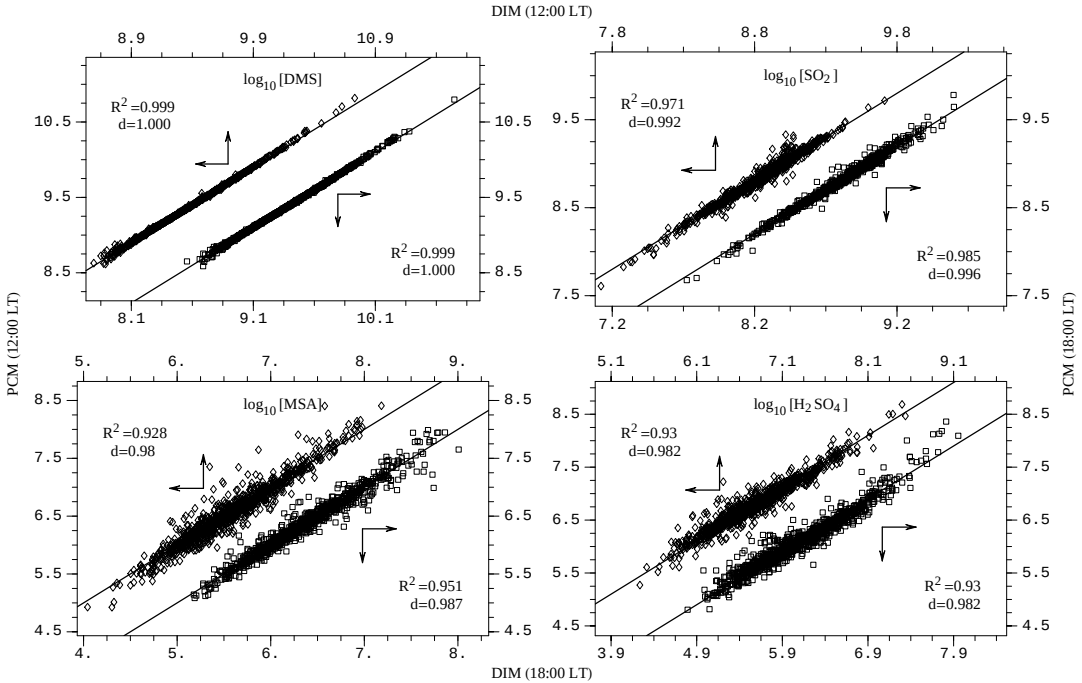

Fig. 3. Correlations between logarithmic concentrations using DIM and PCM. Correlations are displayed at 12:00 LT (diamonds, top/left axes) and 18:00 LT (squares, bottom/right axes) using 10^3 common sets of randomly sampled parameters. Also shown are the 1:1 lines, coefficients of determination (R^2), and indices of agreement (d).

ACPD
4, 6379–6430, 2004

Sensitivities and uncertainties of DMS oxidation in the RMBL

D. D. Lucas and
R. G. Prinn

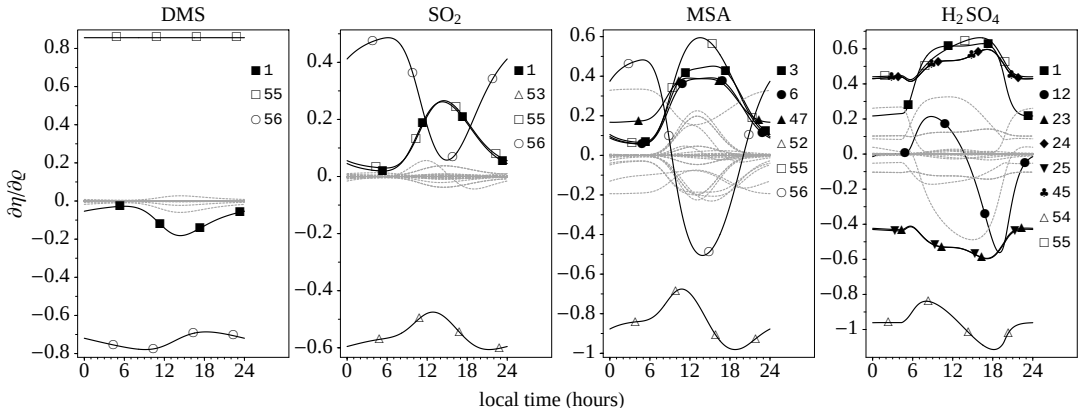

Fig. 4. Diurnal cycles of the first-order normalized sensitivity coefficients for the DMS-related species calculated using Eqs. (6) and (7). The most important sensitivity coefficients are shown by the dark solid lines with individually labeled symbols and parameter numbers on the right. Filled symbols are used for chemical parameters, and empty symbols are used for heterogeneous removal (empty triangle), DMS emissions (empty square), and RMBL mixing (empty circle). The less important sensitivities are shown using gray-dashed lines. Refer to Table 1 for the processes corresponding to the parameter numbers.

ACPD
4, 6379–6430, 2004

Sensitivities and uncertainties of DMS oxidation in the RMBL

D. D. Lucas and R. G. Prinn

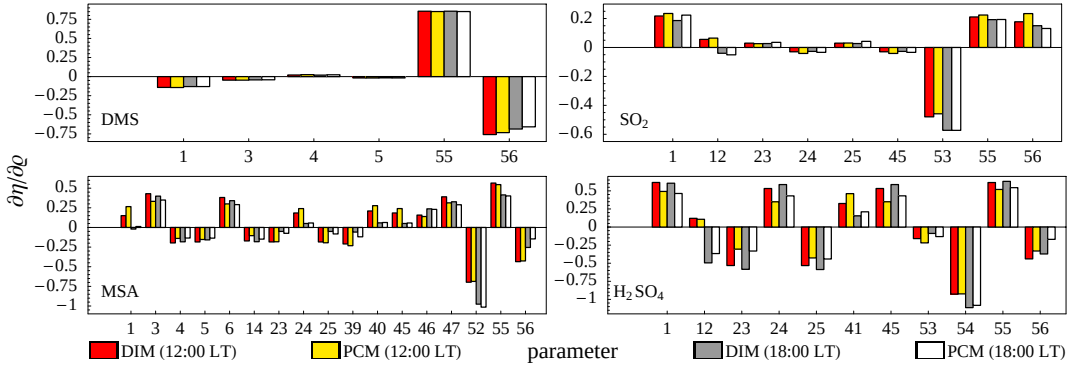

Fig. 5. Comparison of the first-order normalized sensitivity coefficients using DIM (Eqs. 6 and 7) and PCM ($\xi = 0$ in Eq. 8). The sensitivities are compared at 12:00 LT (DIM red, PCM yellow) and 18:00 LT (DIM gray, PCM white). Refer to Table 1 for the parameter labels.

ACPD
4, 6379–6430, 2004

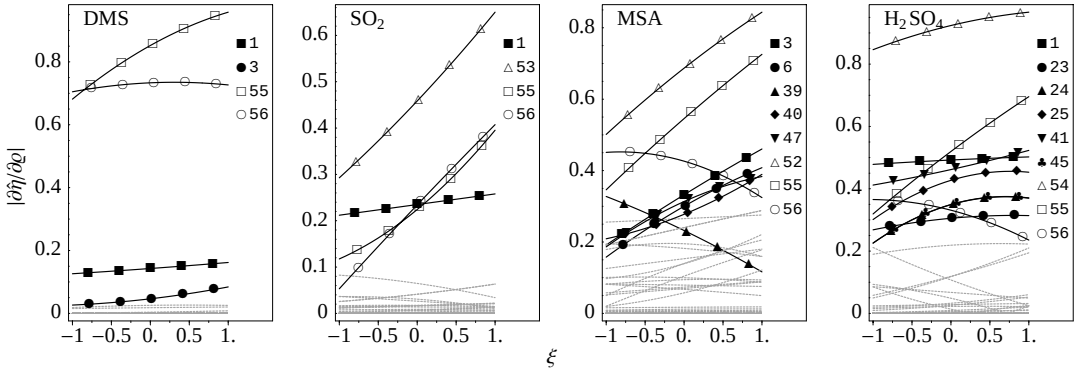

Fig. 6. Magnitudes of the first-order uncertainty-dependent concentration sensitivities as a function of ξ at 12:00 LT. Only the labeled parameter is varied (ξ_q) using Eq. (8) while all other parameters are set to their mean values ($\xi_k = 0$). The most important sensitivities are shown using solid lines and symbols, as noted on the right. Filled symbols are used for chemical parameters, and empty symbols are used for heterogeneous removal (empty triangle), DMS emissions (empty square), and RMBL mixing (empty circle). The less important sensitivities are shown using gray-dashed lines. Refer to Table 1 for the parameter labels.

ACPD
4, 6379–6430, 2004

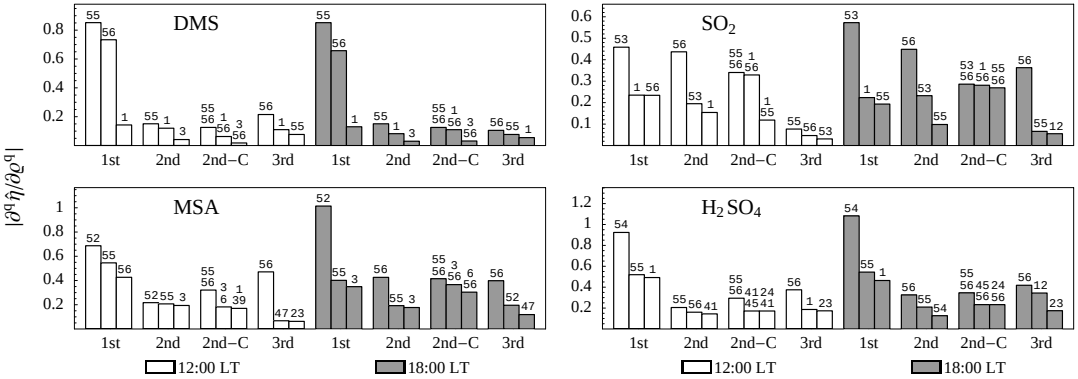

Fig. 7. First-, second-, and third-order sensitivity coefficients for the DMS-related species using PCM at 12:00 LT (white) and 18:00 LT (gray). Second-order cross sensitivities are denoted by 2nd-C. Only the three largest magnitudes of each order are shown. The parameter numbers are noted at the top of each bar, and ξ is set to zero where applicable. Refer to Table 1 for the parameter labels.

ACPD
4, 6379–6430, 2004

Sensitivities and uncertainties of DMS oxidation in the RMBL

D. D. Lucas and R. G. Prinn

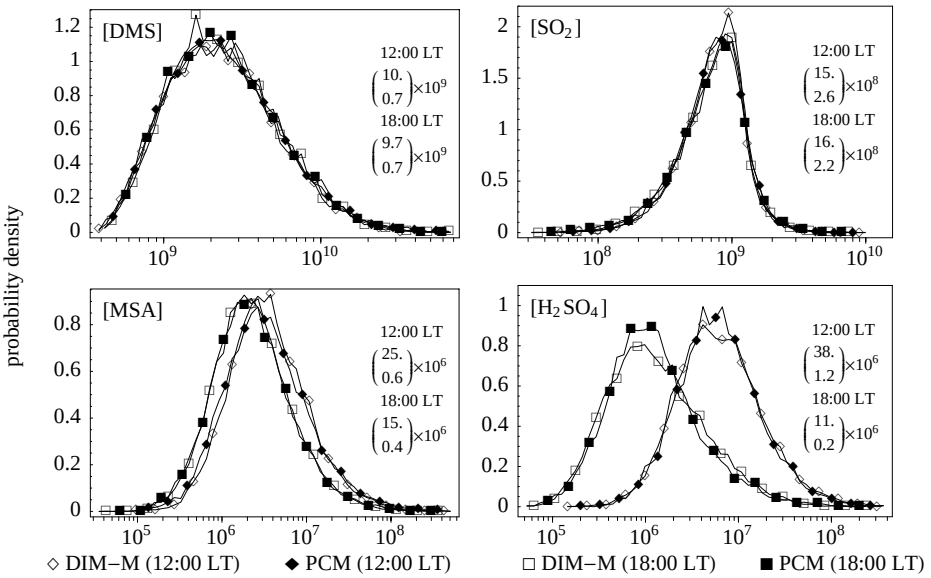

Fig. 8. Probability density functions of the DMS-related concentrations (molecules cm^{-3}) using DIM-M (empty) and PCM (filled) at 12:00 LT (diamonds) and 18:00 LT (squares). Using sample sizes of 10^4, the PDFs were normalized over 50 equally-spaced bins between the minimum and maximum concentrations. Shown on the right are the average 95% confidence limits.

ACPD
4, 6379–6430, 2004

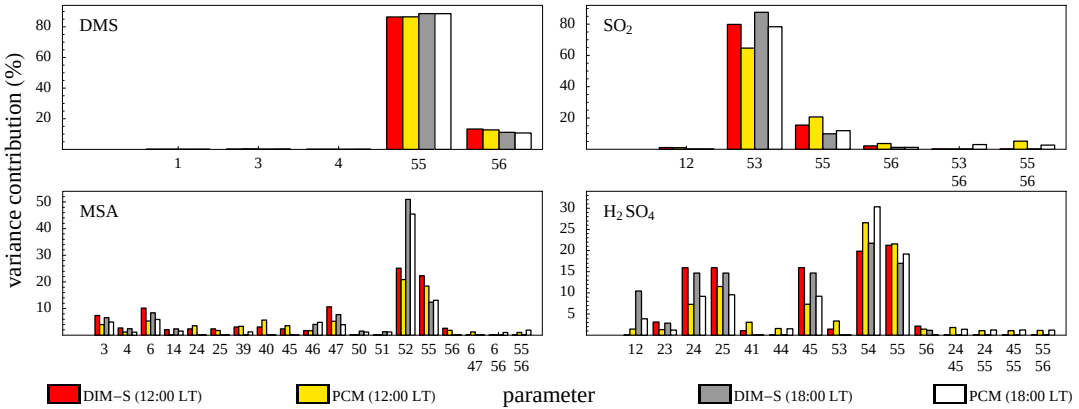

Fig. 9. Parameter variance contributions (%) for the DMS-related species. The contributions are shown at 12:00 LT (DIM-S red, PCM yellow) and 18:00 LT (DIM-S gray, PCM white). Contributions more than 0.05% and 1% are displayed for DMS and the other species, respectively. Contributions from pairs of parameters are also shown. Refer to Table 1 for the parameter labels.

ACPD
4, 6379–6430, 2004

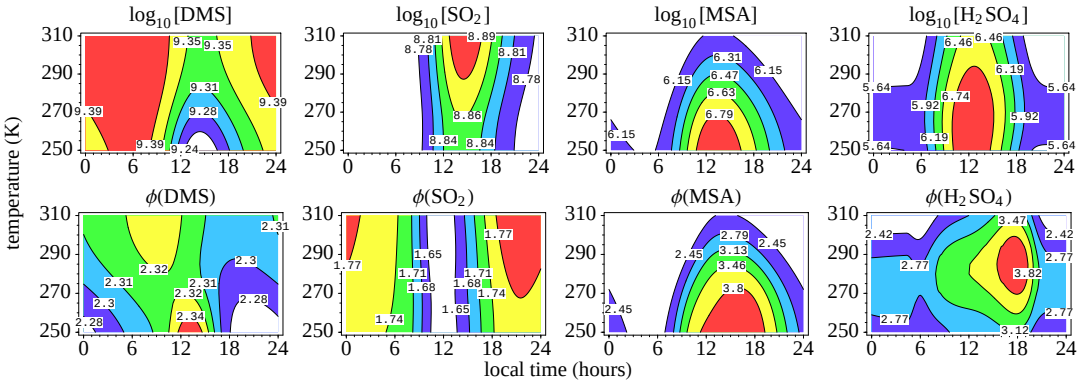

Fig. 10. Time-temperature contours of the logarithmic concentrations (upper) and concentration uncertainties (lower) of the DMS-related species over a daily cycle and temperature range of 250–310 K. The concentration uncertainties are displayed as uncertainty factors (ϕ) using $\log_{10}\phi = \sigma_\eta$, where σ_η is calculated from Eq. (13).

ACPD
4, 6379–6430, 2004

Sensitivities and uncertainties of DMS oxidation in the RMBL

D. D. Lucas and R. G. Prinn